Available online at www.sciencedirect.com
SCIENCE DIRECT®
Comput. Methods Appl. Mech. Engrg. 193 (2004) 1733–1772
Computer methods in applied mechanics and engineering
www.elsevier.com/locate/cma

An introduction and tutorial on multiple-scale analysis in solids

Harold S. Park *, Wing Kam Liu

Department of Mechanical Engineering, Northwestern University, 2145 Sheridan Road, Evanston, IL 60208, USA

Received 2 June 2003; received in revised form 17 August 2003; accepted 2 December 2003

Abstract

Concurrent multiple-scale methods can be defined as those which combine information available from distinct length and time scales into a single coherent, coupled simulation. These methods have recently become both popular and necessary for the following reasons. One is the recent discovery of new, nanoscale materials, and the corresponding boom in nanotechnology research. Another factor is that experiments have conclusively shown the connection between microscale physics and macroscale deformation. Finally, the concept of linking disparate length and time scales has become feasible recently due to the ongoing explosion in computational power.

We present a detailed introduction to the available technologies in the field of multiple-scale analysis. In particular, our review centers on methods which aim to couple molecular-level simulations (such as molecular dynamics) to continuum level simulations (such as finite element and meshfree methods). Using this definition, we first review existing multiple-scale technology, and explain the pertinent issues in creating an efficient yet accurate multiple-scale method. Following the review, we highlight a new multiple-scale method, the bridging scale, and compare it to existing multiple-scale methods. Next, we show example problems in which the bridging scale is applied to fully non-linear problems. Concluding remarks address the research needs for multiple-scale methods in general, the bridging scale method in particular, and potential applications for the bridging scale.

Keywords: Multiple-scale simulations; Bridging scale; Coupling methods; Molecular dynamics; Finite elements; Non-linear

1. Motivation for multi-scale methods

Multi-scale methods are a class of simulation methods that have become useful and important within the past decade. Much of this is due to the fact that the governing physics and mechanics of deforming media have been elucidated over the course of time. Another crucial factor at play is the recent explosion in computational power. When combined, the two factors lead straight towards a new revolution in

* Corresponding author.
E-mail address: hpark@northwestern.edu (H.S. Park).

0045-7825/$ - see front matter © 2004 Elsevier B.V. All rights reserved.
doi:10.1016/j.cma.2003.12.054

computational mechanics, that of multi-scale analysis. A survey of the numerical methods and physics that operate across these disparate length and time scales can be found in [1].

In order to motivate our discussion on multi-scale methods, we use as a model problem that of strain localization, or dynamic shearbanding in metals. Localization problems are well-suited for multi-scale analysis for many reasons. The major reason is because the interesting physics of the problem are concentrated into a small spatial region, i.e. the localized zone. Outside of the localized zone, the behavior of the metal can be well approximated as linear elastic.

Continuum simulations of strain localizations have been successful in certain aspects, and unsuccessful in others. One major shortcoming in numerical simulations of strain localization stems from issues with the finite element method itself. As shown in Fig. 1, the experimentally observed shearband of Zhou et al. [2] propagates in a curved path away from the notch tip. However, were the steel plate to be meshed with finite elements, the shearband would propagate in a direction parallel to the notch tip, see Figs. 2 and 3. This issue was alleviated by the usage of meshfree methods as demonstrated in the work by Li et al. [3]. In that work, the reproducing kernel particle method (RKPM) [4–6] was utilized to successfully reduce mesh alignment sensitivity. A summary of those calculations is shown in Fig. 1.

Another shortcoming with the continuum approach lies in the inability of the constitutive relations to resolve small scale details within the shearband itself. An example of this is the inhomogeneous nature of the temperature profile within a shearband, which was discussed by Guduru et al. [7]. If a continuum model is used to simulate this phenomena, many finite elements are needed in order to resolve the "hot spots", while correspondingly few elements are needed outside of the localized zone. Despite this effort, it is unclear

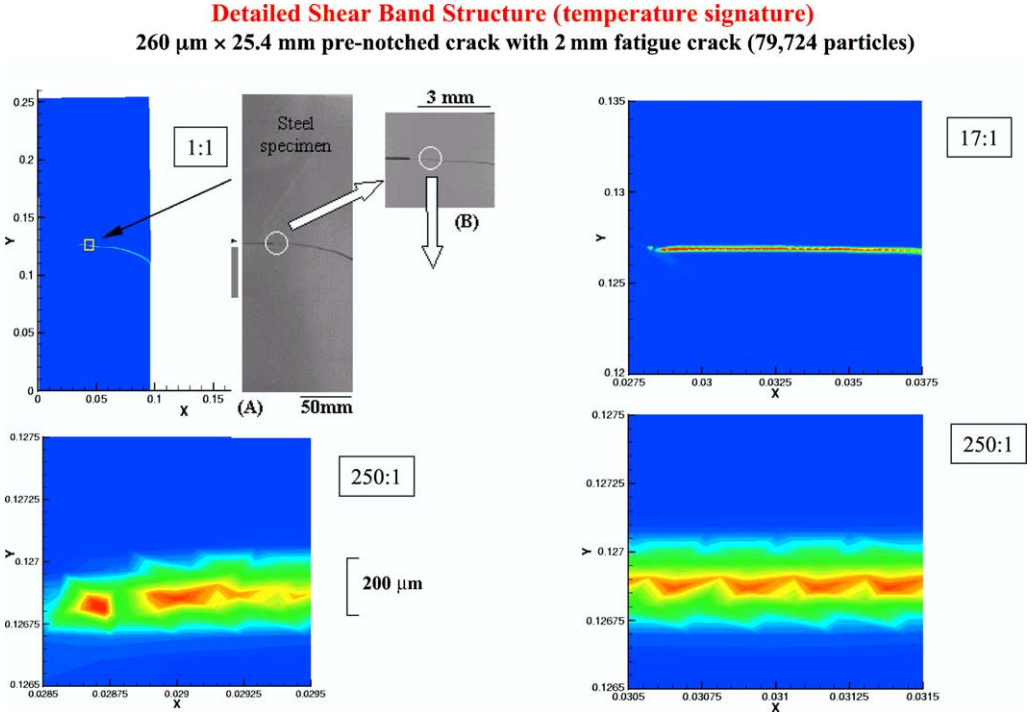

Fig. 1. Comparison of experimental and numerical results. From [3].

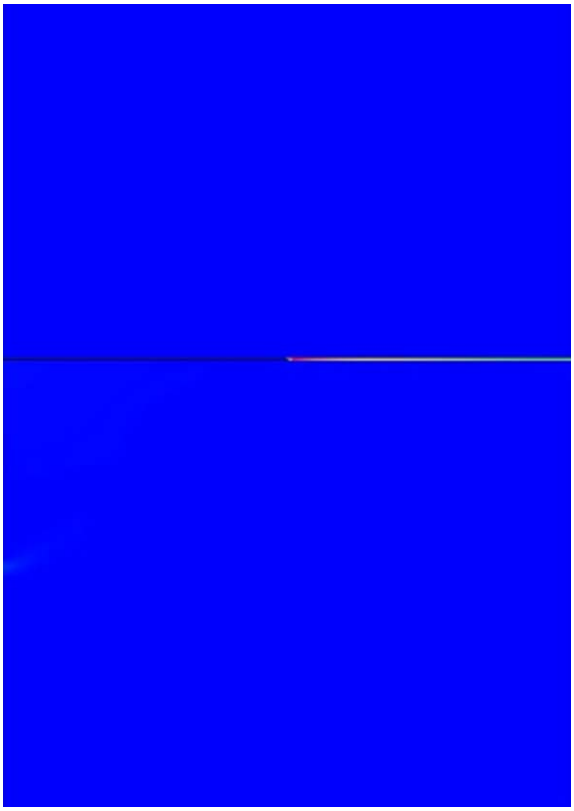

Fig. 2. Effective strain for FEM. Note that shearband propagates parallel to notch for FEM. From [8].

whether a convergent solution can in fact be reached. Thus, it is questionable whether using a continuum approach is the optimal choice, as a great deal of computational expense is necessary for what may not be a physically meaningful or accurate solution.

In contrast, if an atomistic-level simulation were used to model this problem, then the motion of the individual atoms within the localized region could be accurately modeled, presuming the atomic interactions are governed by a suitable potential energy function. Unfortunately, it is currently impossible to model an entire macroscopic domain with atoms, despite the recent advances in computational power. Therefore, a logical solution to this issue is to use a continuum simulation where there is no necessity to accurately model the fine scale physics, to use an atomistic simulation where it is important to model the fine scale physics accurately, and to couple the two simulations in some manner.

We shall continue this article by first reviewing and discussing existing methods which aim to satisfy this goal of coupling continuum and atomistic simulations. To illustrate what has already been done, we show an analytic solution for MD/FE coupling, and show numerical examples for that particular coupling. Next, we review a new multiple-scale method, the bridging scale [9], and discuss a technique to eliminate elastic wave reflection at the MD/FE interface. We verify the bridging scale by showing fully non-linear numerical examples, and demonstrate the effectiveness of truncating the time history kernel for computational efficiency. Finally, we conclude by discussing potential applications for the bridging scale, as well as future research directions.

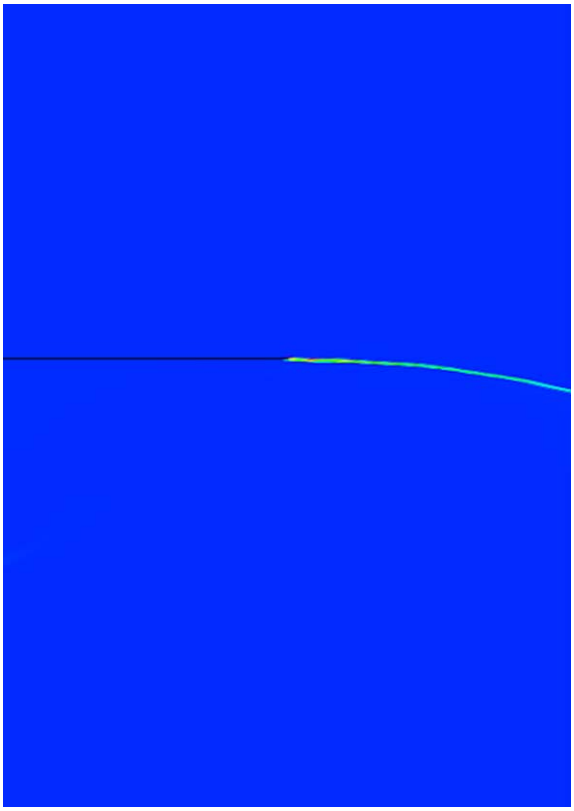

Fig. 3. Effective strain for RKPM. Shearband propagates in curved path using RKPM. From [8].

1.1. MAAD

One pioneering multi-scale approach was the work by Abraham et al. [10]. The idea was to concurrently link tight binding (TB), molecular dynamics (MD) and finite elements (FE) together in a unified approach called MAAD (macroscopic, atomistic, ab initio dynamics). Concurrent linking here means that all three simulations run at the same time, and dynamically transmit necessary information to and receive information from the other simulations. In this approach, the FE mesh is graded down until the mesh size is on the order of the atomic spacing, at which point the atomic dynamics are governed via MD. Finally, at the physically most interesting point, i.e. at a crack tip, TB is used to simulate the atomic bond breaking processes. The interactions between the three distinct simulation tools are governed by conserving energy in the system [11]

$$H_{\mathrm{TOT}} = H_{\mathrm{FE}} + H_{\mathrm{FE/MD}} + H_{\mathrm{MD}} + H_{\mathrm{MD/TB}} + H_{\mathrm{TB}}. \tag{1}$$

More specifically, the Hamiltonian, or total energy of the MD system can be written as

$$H_{\mathrm{MD}} = \sum_{i<j} V^{(2)}(r_{ij}) + \sum_{i,(j<k)} V^{(3)}(r_{ij}, r_{ik}, \Theta_{ijk}) + K, \tag{2}$$

where the summations are over all atoms in the system, K is the kinetic energy of the system, r_{ij} and r_{ik} indicate the distance between two atoms and Θ_{ijk} is the bonding angle between three atoms. The summation

convention $i < j$ is performed so that each atom ignores itself in finding its nearest neighbors. Here the potential energy is comprised of two parts. The first ($V^{(2)}$) is two-body interactions, for example nearest neighbor spring interactions in 1D. The second part are the three-body interactions ($V^{(3)}$), which incorporate such features as angular bonding between atoms. The three-body interactions also make the potential energy of each atom dependent on its environment. The finite element Hamiltonian can be written as the sum of the kinetic and potential energies in the elements, i.e.

$$H_{\mathrm{FE}} = V_{\mathrm{FE}} + K_{\mathrm{FE}}. \tag{3}$$

Expanding these terms gives

$$V_{\mathrm{FE}} = \frac{1}{2}\int_{\Omega} \boldsymbol{\epsilon}(\mathbf{r}) \cdot \mathbf{C} \cdot \boldsymbol{\epsilon}(\mathbf{r})\, \mathrm{d}\Omega, \tag{4}$$

$$K_{\mathrm{FE}} = \frac{1}{2}\int_{\Omega} \rho(\mathbf{r})(\dot{\mathbf{u}})^2\, \mathrm{d}\Omega, \tag{5}$$

where $\boldsymbol{\epsilon}$ is the strain tensor, $\mathbf{C}$ is the stiffness tensor, ρ is the material density and $\dot{\mathbf{u}}$ are the nodal velocities. Thus the potential energy contribution to the FE Hamiltonian V_{FE} is the integral of the strain energy, while the kinetic energy depends upon the nodal velocities. The TB total energy is written as

$$V_{\mathrm{TB}} = \sum_{n=1}^{N_{\mathrm{occ}}} \epsilon_n + \sum_{i<j} V^{\mathrm{rep}}(r_{ij}). \tag{6}$$

This energy can be interpreted as having contribution from an attractive part ϵ_n and a repulsive part V^{rep}. N_{occ} are the number of occupied states. While a detailed overview of tight binding methods is beyond the scope of this work, further details can be found in [12].

The overlapping regions (FE/MD and MD/TB) are termed "handshake" regions, and each makes a contribution to the total energy of the system. The handshake potentials are combinations of the potentials given above, with weight factors chosen depending on whether the atomic bond crosses over the given interface. The three equations of motion (TB/FE/MD) are all integrated forward using the same timestep. This method was applied successfully to the simulation of brittle fracture by Abraham et al. [13].

An approach related to the TB/MD/FE approach of Abraham et al. was developed by Rudd and Broughton [14] called coarse-grained molecular dynamics (CGMD). This approach removes the TB method from the TB/MD/FE method and instead couples only FE and MD. Again, the FE mesh is graded down to the atomistic scale. A key development was that in recognizing that degrees of freedom were missing from the system due to the coarse-graining approximation. A total energy was derived for CGMD using statistical mechanics principles, which is stated to be

$$E(\mathbf{u}_k, \dot{\mathbf{u}}_k) = U_{\mathrm{int}} + \frac{1}{2}\sum_{j,k} (M_{jk}\dot{\mathbf{u}}_j\dot{\mathbf{u}}_k + \mathbf{u}_j K_{jk}\mathbf{u}_k), \tag{7}$$

where $U_{\mathrm{int}} = 3(N - N_{\mathrm{node}})kT$. The energy is comprised of the average kinetic and potential energies as well as a thermal term from the coarse grained (eliminated) degrees of freedom. It was demonstrated that elastic wave reflection measured by a reflection coefficient using CGMD was smaller than the previous TB/MD/FE method of Abraham [14].

1.2. MD/FE coupling—1D example

We now present a theory of coupling FE and MD only. The first crucial point is that *both* the MD and FE systems obey Newton's equations of motion

$$\mathbf{f} = \mathbf{M}\mathbf{a}. \tag{8}$$

Therefore, we must define the force vector $\mathbf{f}$ and mass matrix $\mathbf{M}$ for each system. For an MD system, the force $\mathbf{f}_{\mathrm{MD}}$ is computed by differentiating a potential energy function Φ, which is typically a function of the atomic positions, i.e.

$$\mathbf{f}_{\mathrm{MD}} = -\nabla\Phi(\mathbf{r}_1, \ldots, \mathbf{r}_N), \tag{9}$$

where $\mathbf{r}_i$ is the distance between neighboring atoms. One of the most common interatomic potentials is the Lennard-Jones (LJ) 6-12 potential. The potential energy function for the LJ 6-12 is expressed as

$$\Phi(r_{ij}) = 4\epsilon\left(\left(\frac{\sigma}{r_{ij}}\right)^{12} - \left(\frac{\sigma}{r_{ij}}\right)^{6}\right), \tag{10}$$

where ϵ and σ are constants chosen to fit material properties and r_{ij} is the distance between two atoms i and j. The LJ 6-12 is termed a pair potential because the energy depends only upon the distance r_{ij} between two atoms. The $1/r_{ij}^{12}$ term is meant to model the repulsion between atoms as they approach each other, and is motivated by the Pauli principle in chemistry. The Pauli principle implies that as the electron clouds of the atoms begin to overlap, the system energy increases dramatically because two interacting electrons cannot occupy the same quantum state. The $1/r_{ij}^{6}$ term adds cohesion to the system, and is meant to mimic van der Waals type forces. The van der Waals interactions are fairly weak in comparison to the repulsion term, hence the lower order exponential assigned to the term.

It is crucial to note that the LJ 6-12 is not a realistic potential, because of the pair interaction limitation. In accepting this limitation, the LJ 6-12 is most commonly used in simulations where a general class of effects is studied, instead of specific physical properties, and a physically reasonable yet simple potential energy function is desired. We may now derive the interatomic forces in 1D based on the LJ 6-12 potential by employing (9) to obtain

$$\frac{\partial\Phi}{\partial r_{ij}} = 4\epsilon\left(-12\frac{\sigma^{12}}{r_{ij}^{13}} + 6\frac{\sigma^{6}}{r_{ij}^{7}}\right). \tag{11}$$

The force is then the negative of the gradient of the potential energy. Assuming that $\sigma = 1$ and $\epsilon = 1$, the force f on atom i and is written in simplified form as

$$f_i = -\sum_{i\neq j}\frac{24}{r_{ij}^{7}}\left(1 - \frac{2}{r_{ij}^{6}}\right). \tag{12}$$

The force and potential energy for the LJ 6-12 are shown in Fig. 4. It should be mentioned that the axes of Fig. 4 are in terms of σ and ϵ, which are the LJ parameters. Furthermore, the equilibrium distance between two atoms interacting via a Lennard-Jones relation is $\sqrt[6]{2}\sigma$.

In our 1D coupling example, we assume that these atoms interact with their nearest neighbors via a harmonic potential. The harmonic potential energy can be written as

$$\Phi(r_{ij}) = \tfrac{1}{2}k(r_{ij} - r_0)^2, \tag{13}$$

where k is the spring constant, r_{ij} is the interatomic distance and r_0 is the equilibrium bond length. Taking the negative gradient of Φ with respect to r_{ij} gives the MD force displacement relationship

$$f_i = -k(r_{ij} - r_0), \tag{14}$$

Eq. (14) can be rewritten in a different form by noting the following relationships. First, the equilibrium bond length is the difference in initial positions of two atoms, i.e. $r_0 = x_j - x_i$. The interatomic distance can

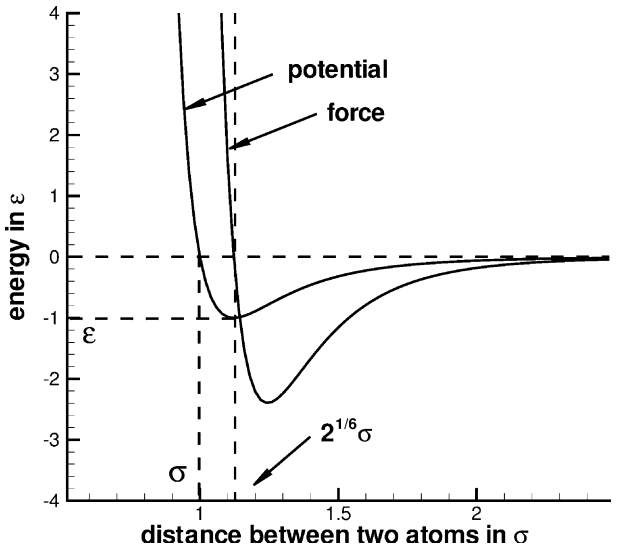

Fig. 4. Force and potential energy plot for Lennard-Jones 6-12 potential.

then be written as a function of the initial positions and the displacements d of each atom as $r_{ij} = x_j + d_j - (x_i + d_i)$. Therefore, $r_{ij} - r_0 = d_j - d_i = \Delta x$, where Δx is the relative displacement between two neighboring atoms. We will use this notation for the remainder of this paper.

A useful analogy can be made by comparing the behavior of the harmonic potential to continuum linear elasticity. Note that unlike the Lennard-Jones potential, the harmonic potential cannot recognize bond breaking or separation, because the force is a continuous function of relative displacement. For the Lennard-Jones potential, the attractive force dies out quickly after about two interatomic distances, which allows bond breaking if the tensile force is strong enough. In this sense, the harmonic potential is akin to linear elasticity on the atomic level.

The mass matrix $\mathbf{M}_{\mathrm{MD}}$ is a diagonal matrix with the individual atomic masses on the diagonal. For a two atom system, this would look as follows:

$$\mathbf{M}_{\mathrm{MD}} = \begin{pmatrix} m_1 & 0 \\ 0 & m_2 \end{pmatrix}, \tag{15}$$

where m_i are the masses of each individual atom. At this point, all the information needed to solve the equation of motion for the MD system has been defined, and we move onto defining the necessary finite element quantities. For a finite element system, the mass matrix $\mathbf{M}_{\mathrm{FE}}$ can be defined as follows:

$$\mathbf{M}_{\mathrm{FE}} = \int_{\Omega_0} \rho_0 \mathbf{N}^{\mathrm{T}} \mathbf{N} \, \mathrm{d}\Omega_0, \tag{16}$$

where ρ_0 is the initial material density, Ω_0 is the undeformed volume and $\mathbf{N}$ are the finite element shape functions, which are typically low order polynomials. If linear shape functions are used, the lumped mass matrix for a single element can be written as

$$\mathbf{M}_{\mathrm{FE}} = \frac{\rho_0 A_0 l_0}{2} \begin{pmatrix} 1 & 0 \\ 0 & 1 \end{pmatrix}, \tag{17}$$

where A_0 is the initial area of the finite element and l_0 is the initial length of the finite element. Eq. (17) states that half the mass in the finite element is assigned to each node. We use the lumped mass matrix in the following 1D MD/FE coupling example to preserve the diagonal quality of the global mass matrix.

For the FE force $\mathbf{f}_{\mathrm{FE}}$, we shall assume that no external forces act upon the system, so that $\mathbf{f}_{\mathrm{FE}} = \mathbf{f}_{\mathrm{FE}}^{\mathrm{int}}$, or the total force is equal to the internal force $\mathbf{f}_{\mathrm{FE}}^{\mathrm{int}}$. The internal force in an FE simulation is computed by multiplying the stiffness $\mathbf{K}$ by the nodal displacements $\mathbf{d}$

$$\mathbf{f}_{\mathrm{FE}} = \mathbf{K}_{\mathrm{FE}}\mathbf{d}. \tag{18}$$

For a linear elastic system, the stiffness matrix takes the familiar form

$$\mathbf{K}_{\mathrm{FE}} = \frac{-kh_a}{l_0}\begin{pmatrix} 1 & -1 \\ -1 & 1 \end{pmatrix} \tag{19}$$

if it is assumed that the smallest element, i.e. that with nodal spacing equal to the atomic spacing h_a, acts as the parent element. The preceding finite element equations are derived and explained in detail in the text by Belytschko and Moran [15].

1.2.1. Derivation of coupled FE/MD equations of motion

The key point now is to couple the MD and FE systems. Suppose that there is one finite element in which the nodes exactly overlap the MD atoms. We refer to this as the "handshake" element. The question for this element is how to define the mass matrix and force vector. For the mass matrix, the procedure described above for (17) can be used. For the force vector, a different method must be utilized. The method used is to weight the contribution to the total force between the MD force and FE force. In this case, because the nodes and atoms overlap exactly, it is determined that the total force is equally weighted from the MD force and FE force.

In detail, the interaction force $\mathbf{f}_{\mathrm{MD}}$ is calculated for the two "handshake" atoms, which are atoms 2 and 3 in Fig. 5. The force vector components f_2 and f_3 are then augmented as follows:

$$f_2 = f_2 + \tfrac{1}{2}f_{\mathrm{MD}}, \tag{20}$$

$$f_3 = f_3 + \tfrac{1}{2}f_{\mathrm{MD}}. \tag{21}$$

Because only half the MD force makes a contribution to the total force, the other half must come from the FE internal force. This contribution is made in the same manner as above. First, the FE force f_{FE} is computed for the boundary element

$$f_2 = f_2 + \tfrac{1}{2}f_{\mathrm{FE}}, \tag{22}$$

$$f_3 = f_3 + \tfrac{1}{2}f_{\mathrm{FE}}. \tag{23}$$

If the FE region does not exactly overlap the boundary MD region, different weighting combinations can be used.

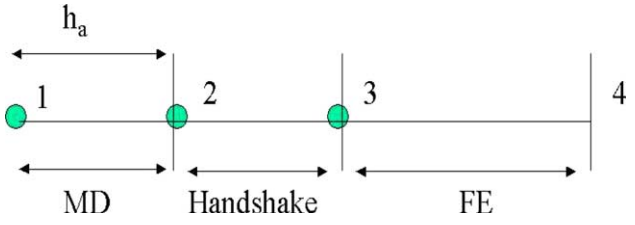

Fig. 5. Problem description for 1D MD/FE coupling.

For the three atom, two element (the handshake region counts as an element) example shown in Fig. 5, we now derive the coupled MD/FE equations of motion. The atoms are assumed to have mass m, as do both finite elements. The atomic spacing is h_a, as is the nodal spacing for both finite elements, which implies that the first finite element after the handshake element also has a nodal spacing which equals the interatomic spacing. The displacements of the atoms/nodes are assumed to be d_1, d_2, d_3 and d_4. Because the masses of the atoms and finite elements are equal, we can write the mass matrix $\mathbf{M}$ for this system as

$$\mathbf{M} = \begin{pmatrix} m & 0 & 0 & 0 \\ 0 & m & 0 & 0 \\ 0 & 0 & m & 0 \\ 0 & 0 & 0 & m \end{pmatrix}. \tag{24}$$

We now turn to the details of constructing the force vector. For the first pair of atoms, the force can be written as

$$\mathbf{f} = -k\,\Delta\mathbf{x} = -k(d_2 - d_1), \tag{25}$$

where d_i are the displacements of each atom. The force is apportioned to each atom so the force vector is written as

$$\mathbf{f} = \begin{pmatrix} k(d_2 - d_1) \\ -k(d_2 - d_1) \\ 0 \\ 0 \end{pmatrix}. \tag{26}$$

Note that the sum of the forces is zero. For the finite element with nodes 3 and 4, the force is calculated by multiplying the stiffness matrix by the displacements,

$$\begin{pmatrix} f_3 \\ f_4 \end{pmatrix} = -\frac{kh_a}{l_0} \begin{pmatrix} 1 & -1 \\ -1 & 1 \end{pmatrix} \begin{pmatrix} d_3 \\ d_4 \end{pmatrix}. \tag{27}$$

Adding this to the global force vector $\mathbf{f}$ gives

$$\mathbf{f} = \begin{pmatrix} k(d_2 - d_1) \\ -k(d_2 - d_1) \\ k(d_4 - d_3) \\ -k(d_4 - d_3) \end{pmatrix}. \tag{28}$$

Finally, the handshake region comprised of atoms/nodes 2 and 3 are considered. Because the FE nodes and MD atoms coincide for this case, it is assumed that each will contribute half of the total force. Mathematically, this says

$$\begin{pmatrix} f_2 \\ f_3 \end{pmatrix} = \frac{1}{2} \begin{pmatrix} f_{\mathrm{MD2}} \\ f_{\mathrm{MD3}} \end{pmatrix} + \frac{1}{2} \begin{pmatrix} f_{\mathrm{FE2}} \\ f_{\mathrm{FE3}} \end{pmatrix}. \tag{29}$$

The MD forces are

$$\begin{pmatrix} f_{\mathrm{MD2}} \\ f_{\mathrm{MD3}} \end{pmatrix} = \frac{k}{2} \begin{pmatrix} d_3 - d_2 \\ -(d_3 - d_2) \end{pmatrix}, \tag{30}$$

while the FE forces are

$$\begin{pmatrix} f_{\mathrm{FE2}} \\ f_{\mathrm{FE3}} \end{pmatrix} = \frac{k}{2} \begin{pmatrix} d_3 - d_2 \\ -(d_3 - d_2) \end{pmatrix}. \tag{31}$$

Because the linear spring assumption is used for both the MD and FE systems, the MD forces are identical to the FE forces for this case. Thus, the complete system of equations for this three-atom, two element system reads

$$\begin{pmatrix} m & 0 & 0 & 0 \\ 0 & m & 0 & 0 \\ 0 & 0 & m & 0 \\ 0 & 0 & 0 & m \end{pmatrix} \begin{pmatrix} \ddot{d}_1 \\ \ddot{d}_2 \\ \ddot{d}_3 \\ \ddot{d}_4 \end{pmatrix} = \begin{pmatrix} k(d_2 - d_1) \\ k(d_3 - 2d_2 + d_1) \\ k(d_4 - 2d_3 + d_2) \\ k(d_3 - d_4) \end{pmatrix}. \tag{32}$$

1.2.2. MD/FE coupling numerical examples

To further illustrate the direct coupling of FE and MD, we present a simplified 1D example of MAAD including coupling between finite elements and molecular dynamics, but excluding tight binding. The problem description is shown pictorially in Fig. 6. The problem is symmetric about $x = 0$, as the MD region has 101 atoms from $x = -2$ to 2. The finite element region has 100 elements. Fifty elements are used between $x = -10$ and -1.96, and 50 elements are used between $x = 1.96$ and 10. Thus there are two handshake regions in which the atomistic positions and the finite element nodes coincides. The first is the finite element with nodes at $x = -2$ and -1.96. The second is the finite element with nodes at $x = 1.96$ and 2.

As was mentioned above, only one system of equations is solved. Therefore, all the degrees of freedom are integrated forward in time using the same time integration algorithm. Typically for MD, a velocity Verlet or Gear sixth order time integrator is used. Literature covering these topics can be found in [16]. In our example, the equations of motion are integrated forward in time using Ruth's symplectic leapfrog algorithm [16]. This is a two-stage algorithm to update the velocities and displacements and is implemented as follows:

$$\mathbf{v}_1 = \mathbf{v}_0, \tag{33}$$

$$\mathbf{d}_1 = \mathbf{d}_0 + \tfrac{1}{2}\mathbf{v}_1 \Delta t, \tag{34}$$

$$\mathbf{v}_2 = \mathbf{v}_1 + \mathbf{f}(\mathbf{d}_1)\Delta t, \tag{35}$$

$$\mathbf{d}_2 = \mathbf{d}_1 + \tfrac{1}{2}\mathbf{v}_2 \Delta t. \tag{36}$$

The 0 subscripts indicate initial values, the 1 subscripts indicate values after the first stage, and the 2 subscripts are the values at the end of the timestep. The key point is that the force $\mathbf{f}$ is evaluated only once, which is crucial since the force calculation is the most expensive part of an MD simulation. The remaining parts of the two-stage update require little memory and computational expense.

A gaussian-type wave which is symmetric about $x = 0$ is applied to the MD system. The initial configuration of the problem is shown in Fig. 7. Two cases were tested. In the first case, all the finite elements

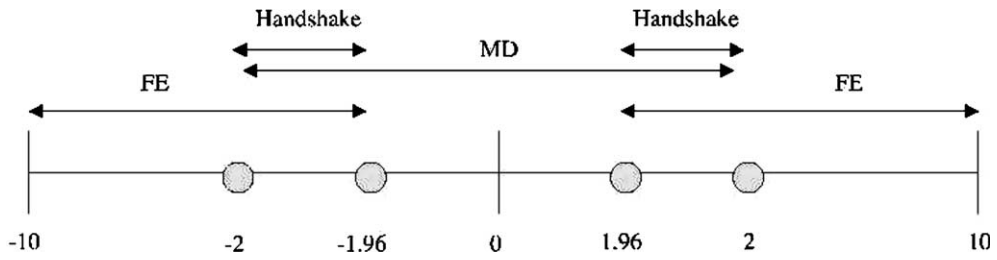

Fig. 6. Problem description for 1D MD/FE coupling.

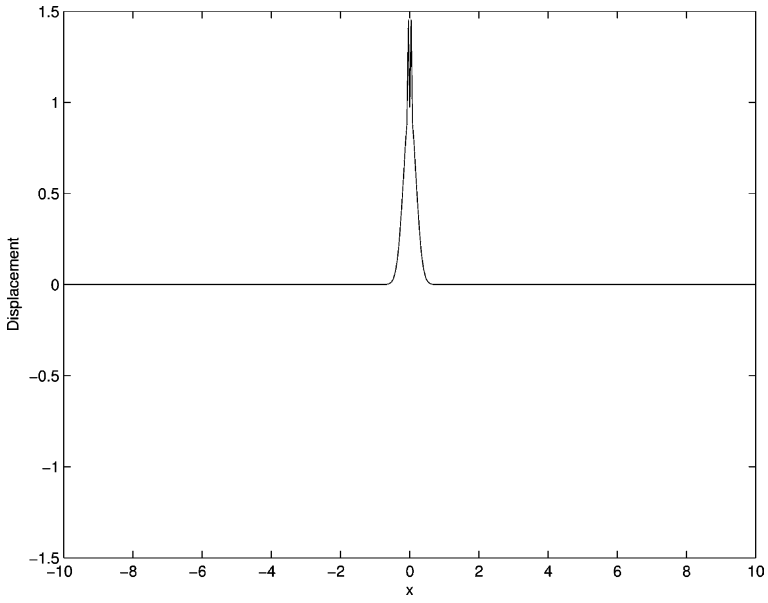

Fig. 7. Initial displacement for 1D FE/MD coupled problem.

had the same spacing as the atomic spacing. In the second case, the FE nodal spacing increased with the distance from the MD region. The atomic masses and spring constant were taken to be unity.

In the first case, as depicted in Fig. 8, because the FE nodal spacing is the same as the atomic spacing everywhere, the coupled equations of motion are identical, and the wave sees the same system whether it is passing through the MD or FE regions. Thus, the transition from the MD to FE region is smooth as well, and no wave reflection occurs. In contrast, as shown in Fig. 9, if the FE mesh is graded as the distance from the MD region increases, wave reflection is immediately noticeable in the MD region. Due to the fact that the finite elements are unable to resolve the small wavelengths coming from the MD region, and because the formulation is energy conserving, the waves must go somewhere and are thus reflected back into the MD region.

1.3. Quasi-continuum method and Cauchy–Born rule

A different approach to multi-scale modeling, the quasi-continuum method, was developed by Tadmor et al. [17]. The atomistic to continuum link is achieved here by the use of the Cauchy–Born rule. The Born rule assumes that the continuum energy density W can be computed using an atomistic potential, with the link to the continuum being the deformation gradient $\mathbf{f}$. To briefly review continuum mechanics, the deformation gradient $\mathbf{f}$ maps an undeformed line segment $d\mathbf{X}$ in the reference configuration onto a deformed line segment $d\mathbf{x}$ in the current configuration

$$d\mathbf{x} = \mathbf{F}\, d\mathbf{X}. \tag{37}$$

In general, $\mathbf{F}$ can be written as

$$\mathbf{F} = 1 + \frac{d\mathbf{u}}{d\mathbf{X}}, \tag{38}$$

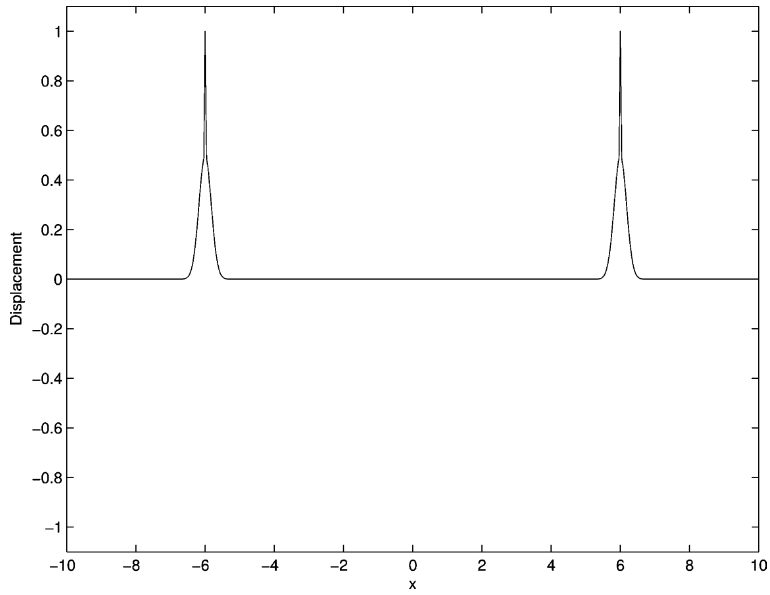

Fig. 8. Snapshot of displacement for 1D FE/MD coupled problem after wave has propagated into the FE region for case where FE nodal spacing equals atomic spacing everywhere.

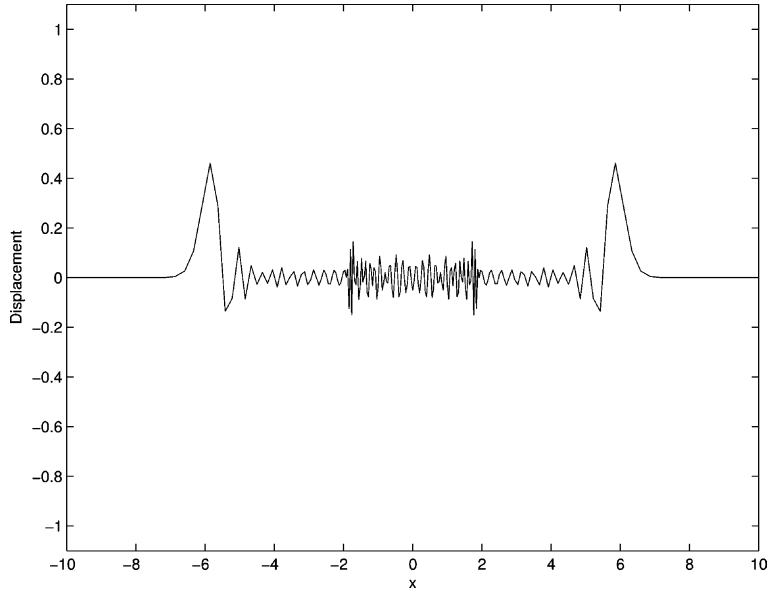

Fig. 9. Snapshot of displacement for 1D FE/MD coupled problem after wave has propagated into the FE region for case where FE nodal spacing gradually increases with distance from MD region.

where **u** is the displacement. If there is no displacement in the continuum, the deformation gradient is equal to unity.

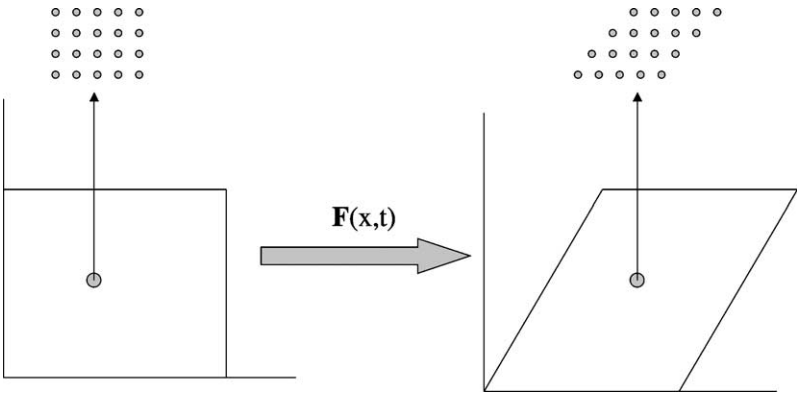

Fig. 10. Illustration of Cauchy–Born rule.

The major restriction and implication of the Cauchy–Born rule is that the continuum deformation must be homogeneous. This results from the fact that the underlying atomistic system is forced to deform according to the continuum deformation gradient **F**, as is illustrated in Fig. 10. By using the Born rule, the authors were able to derive a continuum stress tensor and tangent stiffness directly from the interatomic potential, which allowed the usage of the standard non-linear finite element method. This can be done by the following relations

$$\mathscr{P} = \frac{\partial W}{\partial \mathbf{F}^{\mathrm{T}}}, \tag{39}$$

$$\mathbf{C} = \frac{\partial^2 W}{\partial \mathbf{F}^{\mathrm{T}} \partial \mathbf{F}^{\mathrm{T}}}, \tag{40}$$

where **C** is the Lagrangian tangent stiffness and $\mathscr{P}$ is the first Piola–Kirchoff stress tensor.

Adaptativity criteria were used in regions of large deformation so that full atomic resolution could be achieved in these instances, i.e. near a dislocation. A non-local version of the Born rule was also developed so that non-homogeneous deformations such as dislocations could be modeled. The quasi-continuum method has been applied to quasi-static problems such as nanoindentation [18].

Other related multi-scale approaches include that of Arroyo and Belytschko [19]. In this approach, a correction to the Born rule, the exponential map, was derived for application to the modeling of carbon nanotubes. It was shown that the exponential map made the Born rule valid for nanotube analysis. A similar approach was developed by Huang [20]. Extensions and analysis of the quasi-continuum method were performed by Diestler [21] and Shilkrot et al. [22].

1.3.1. Cauchy–Born rule for linear springs

Two 1D examples are now done to illustrate how the Cauchy–Born rule is used. In the first case, we consider a quadratic potential energy function, which when minimized yields a linear spring force relation. The potential energy Φ is written as

$$\Phi = \tfrac{1}{2} k \Delta x^2, \tag{41}$$

where k is the spring constant and $\Delta \mathbf{x}$ is the relative displacement between two atoms. Differentiating this energy function with respect to the relative displacement yields the MD force

$$f_{\mathrm{MD}} = -\frac{\partial \Phi}{\partial \Delta x} = -k\,\Delta x. \tag{42}$$

In order to use the Cauchy–Born rule, we must make two modifications to (41). The first is to write Φ as a function of the deformation gradient F. The second is to modify the potential energy function Φ such that we can obtain the energy density W. In 1D, we can obtain the energy density directly by dividing the potential energy by the initial atomic bond length. This may be written as

$$W = \frac{\Phi}{r_0}, \tag{43}$$

where r_0 is the initial atomic bond length. One important property that must be conserved in using the Cauchy–Born rule is that the energy of the molecular system must equal the energy in the continuum system, which can be obtained by integrating the energy density and setting it equal to the summation of the bond energies

$$\sum_{i=1}^{\mathrm{nbond}} \Phi_{\mathrm{bond}} = \int_{\Omega_0} W\,\mathrm{d}X. \tag{44}$$

To illustrate (44) via example, consider a three-atom molecular system with initial bond length r_0 and interacting by linear springs of stiffness k. The equivalent continuum system is then of length $2r_0$. This is shown in Fig. 11. The energy in the MD system is computed to be

$$E_{\mathrm{MD}} = 2(\tfrac{1}{2}k\,\Delta x^2) = k\,\Delta x^2. \tag{45}$$

In order to write the continuum energy density as a function of F, we note that using (37), the undeformed bond length r_0 can be related to the deformed bond length r through the deformation gradient by the relation

$$r = Fr_0. \tag{46}$$

The relative displacement Δx can then be written as a function of the deformation gradient F as

$$\Delta x = r_0(F-1). \tag{47}$$

The expression for the continuum energy density becomes, by substituting (47) into (41) and normalizing by the initial bond length

$$W = \frac{1}{r_0}\left(\frac{1}{2}k(r_0(F-1))^2\right). \tag{48}$$

Integrating over the continuum body of length $2r_0$ gives the energy of the continuum system

$$E_{\mathrm{CB}} = kr_0^2(F-1)^2. \tag{49}$$

If the continuum system is stretched to length $4r_0$, $F = 2$, and the continuum energy evaluates to $E_{\mathrm{CB}} = kr_0^2$. The corresponding MD system energy is then obtained by evaluating (45), and yields the same as the continuum energy, $E_{\mathrm{MD}} = kr_0^2$. It is *crucial* to note that in obtaining the MD energy, we assumed that the deformation of each bond was identical. This is a result of the homogeneous deformation assumption that

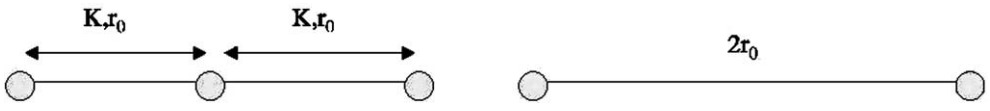

Fig. 11. Three-atom system interacting via linear springs along with homogenized continuum.

underlies the Cauchy–Born rule, i.e. that the underlying atomistic system deforms homogeneously like the continuum system.

In order to now use the Cauchy–Born rule in a finite element formulation, we use (39) and apply it to (48). Differentiating (48) with respect to F gives the expression for the Cauchy–Born force (in 1D, stress and force are equivalent)

$$f_{\mathrm{CB}} = kr_0(F-1). \tag{50}$$

1.3.2. Cauchy–Born rule for Lennard-Jones 6-12 potential

Our second example utilizes a standard non-linear interatomic potential, the Lennard-Jones 6-12 potential. As was previously given in (12), the MD force for the LJ 6-12 potential can be written as

$$f_{\mathrm{MD}} = 48\epsilon\frac{\sigma^{12}}{r^{13}} - 24\epsilon\frac{\sigma^{6}}{r^{7}}. \tag{51}$$

In order to derive the Cauchy–Born force for the LJ 6-12 potential, we again write an expression for the energy density W. Doing so, we obtain

$$W = \frac{1}{r_0}4\epsilon\left(\left(\frac{\sigma}{r}\right)^{12} - \left(\frac{\sigma}{r}\right)^{6}\right). \tag{52}$$

Substituting (46) into (52) and minimizing W with respect to F, we obtain the Cauchy–Born force for the LJ 6-12 potential

$$f_{\mathrm{CB}} = \frac{24\epsilon\sigma^{6}}{F^{7}r_0^{7}} - \frac{48\epsilon\sigma^{12}}{F^{13}r_0^{13}}. \tag{53}$$

One fact which becomes clear in 1D is that the *only* difference between the Cauchy–Born and MD force expression for the same atomic spacing lies in the ability of the finite element simulation to accurately calculate the deformation gradient. If the deformation gradient is calculated exactly and the finite element spacing equals the atomic spacing, then $f_{\mathrm{CB}} = -f_{\mathrm{MD}}$. In practice, however, the deformation gradient is calculated numerically using finite element shape functions, i.e.

$$F = 1 + \frac{\mathrm{d}\mathbf{u}}{\mathrm{d}\mathbf{X}}. \tag{54}$$

In finite elements, the displacement field $\mathbf{u}$ is approximated by shape functions which interpolate nodal values, i.e.

$$\mathbf{u} = \sum_I \mathbf{N}_I(\mathbf{X})\mathbf{d}_I, \tag{55}$$

where $\mathbf{d}_I$ are the nodal displacements and $\mathbf{N}_I(\mathbf{X})$ are the shape functions, which are functions of space and are typically low order polynomials. Substituting (55) into (54), one obtains the numerical form of F

$$F = 1 + \sum_I \frac{\mathrm{d}\mathbf{N}_I}{\mathrm{d}\mathbf{X}}\mathbf{d}_I. \tag{56}$$

Clearly, the quality of the shape function derivatives controls the accuracy to which the deformation gradient can be calculated numerically, and hence controls the accuracy to which the Cauchy–Born rule can mimic the actual MD forces. In 1D, F is a constant for each finite element. Therefore, F can be calculated *exactly* using linear shape functions, as the derivatives of the shape functions will be constants, and thus matches the order of F. Thus in 1D, if the finite element spacing is the same as the atomic spacing, the force

computed using the Cauchy–Born rule will be exactly the negative of the force computed using an interatomic potential.

In the finite element formulation, the first Piola–Kirchoff stress $\mathscr{P}$ is used in the calculation of the internal force $\mathbf{f}^{\text{int}}$, which is defined as

$$\mathbf{f}^{\text{int}} = \int_{\Omega} \mathbf{B}^{\mathrm{T}} \mathscr{P} \, \mathrm{d}\Omega, \tag{57}$$

where $\mathbf{B}$ is the gradient of the shape function matrix $\mathbf{N}$. $\mathbf{B}$ is also referred to as the strain–displacement matrix. If it is assumed that no external force acts upon the system, the semi-discrete finite element equations of motion can be written as

$$\mathbf{M}\ddot{\mathbf{d}} = -\mathbf{f}^{\text{int}}, \tag{58}$$

where $\mathbf{M}$ is the finite element mass matrix and $\ddot{\mathbf{d}}$ are the nodal accelerations, or the second derivatives of the nodal displacements with respect to time. If the internal force is calculated numerically by summing over a discrete set of quadrature points at locations $\mathbf{X}_q$, the FE semi-discrete equations of motion can be expressed as

$$\mathbf{M}\ddot{\mathbf{d}} = -\sum_{q} \frac{\mathrm{d}\mathbf{N}_I}{\mathrm{d}\mathbf{X}}(\mathbf{X}_q)\mathscr{P}(\mathbf{X}_q) w_q, \tag{59}$$

where w_q are the integration weights associated with point $\mathbf{X}_q$. In practice, then, because the FE internal force term involves the negative of the Cauchy–Born stress (or force in 1D), if the FE nodal spacing equals the atomic spacing, the MD and FE equations of motion see the same absolute value of the internal force. Therefore, the only difference between the two simulations is the mass matrix used; in MD, a diagonal mass matrix is used. In FE, a consistent mass matrix is used, though a lumped mass matrix can also be used as was described above. If the FE lumped mass matrix is used and the FE nodal spacing equals the atomic spacing, then the MD and FE displacements are essentially identical.

1.3.3. Cauchy–Born numerical examples

A simple 1D example problem has been run using the LJ 6-12 potential energy function to calculate the first Piola–Kirchoff stress in the finite element formulation. The LJ potential parameters $\sigma = \epsilon = 1$, such that the equilibrium atomic spacing was $r_0 = 2^{\frac{1}{6}}$. Two hundred and one finite element nodes and atoms were used, and were initially spaced at the equilibrium atomic spacing r_0. The problem is symmetric about $x = 0$, hence only the results for $x > 0$ are shown. The FE nodes and MD atoms were given the same initial displacement in the form of a gaussian-type wave with a fine scale perturbation. The initial MD configuration is shown in Fig. 12, and the result after 100 timesteps is shown in Fig. 13. The corresponding FE configuration after 100 timesteps is shown in Fig. 14.

As can be seen by comparing Figs. 13 and 14, the displacements calculated are nearly identical for the FE/Cauchy–Born and MD cases for the LJ 6-12 potential when the finite element nodal spacing is the same as the atomic spacing. This result agrees with the theoretical results discussed above. To further illustrate the Cauchy–Born rule, the same problem description was run, except using a FE nodal spacing of $10r_0$ was used, which means that 20 finite elements were used instead of 200. The configuration after six timesteps is shown in Fig. 15. As can be seen, even with the coarser finite element mesh, the major features of the gaussian wave are captured. This example also illustrates one major shortcoming in using the Cauchy–Born rule, in that the coarse FE mesh does not allow resolution of the fine atomistic details that are available from a full MD simulation. In using the coarser FE mesh here, because many fewer elements are used, the timestep needed is correspondingly larger, and is in fact five times larger than the MD timestep. This illustrates one major advantage of using the Cauchy–Born rule, in that the computational expense

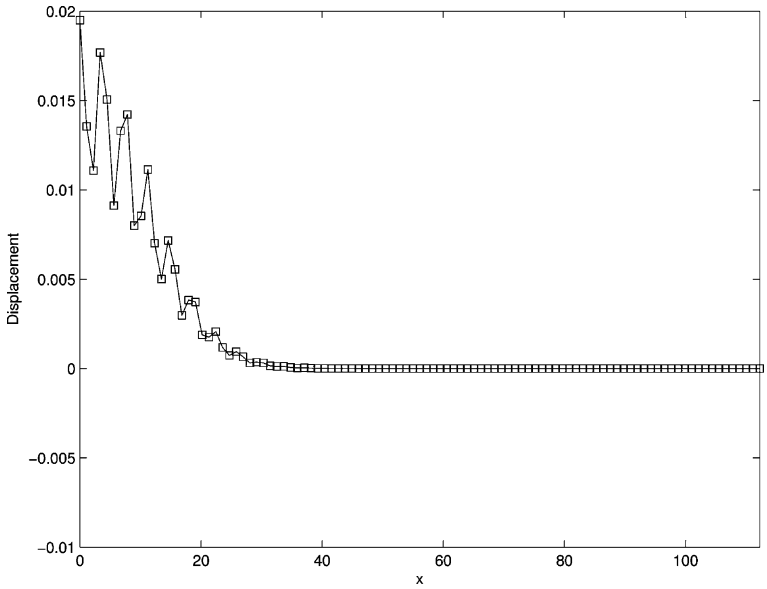

Fig. 12. Initial MD configuration for Cauchy–Born example.

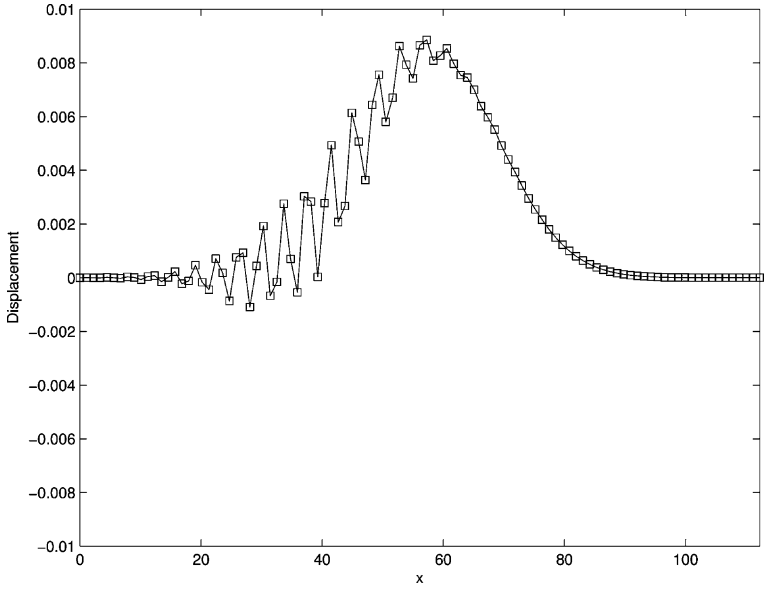

Fig. 13. MD displacements after 100 timesteps.

necessary to obtain a comparable solution to MD is much smaller, due to the smaller number of timesteps and finite elements necessary.

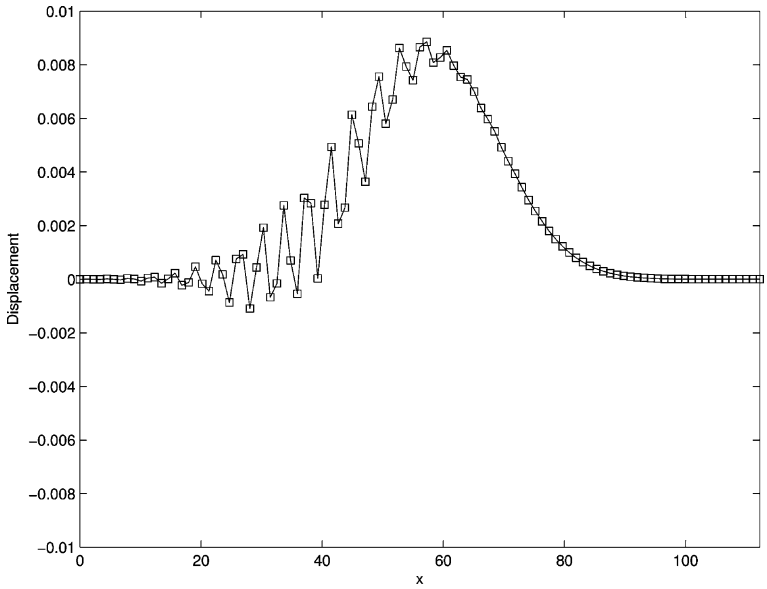

Fig. 14. Left: FE nodal displacements after 100 timesteps.

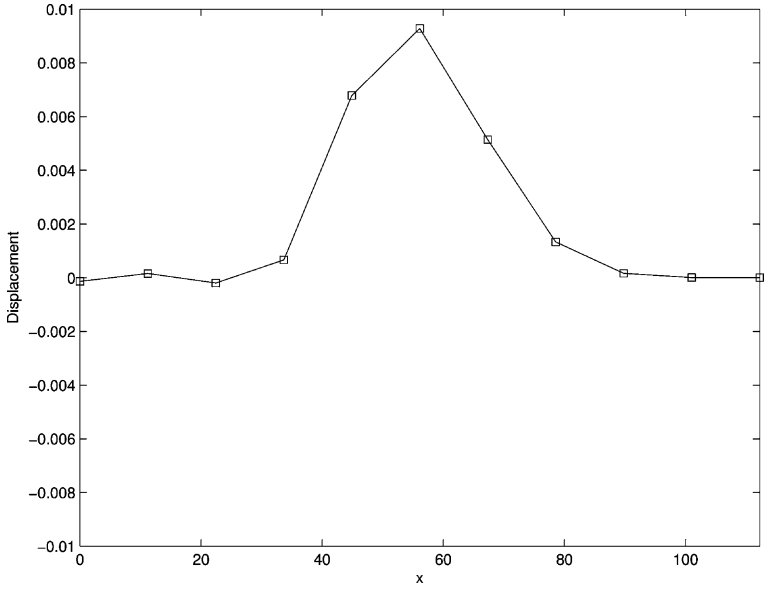

Fig. 15. Right: FE nodal displacements after six timesteps, reduced mesh size.

1.4. Multi-scale issues

There is considerable challenge in developing an efficient yet accurate multi-scale method. One issue is the necessity of meshing the FE region down to the atomic scale. This presents two problems, one numerical and one physical. The numerical issue is that the timestep in an FE simulation is governed by the

smallest element in the mesh. Thus, if the finite elements are meshed down to the atomic scale, many timesteps will be wasted simulating the dynamics in these regions. Furthermore, it seems unphysical that the variables of interest in the continuum region should evolve at the same time scales as the atomistic variables. Thus, a multi-scale method that could incorporate larger timesteps for the continuum region would constitute a significant improvement in this area.

The physical issue in meshing the FE region down to the atomic scale lies in the FE constitutive relations. The constitutive relations typically used in FE calculations, e.g. for plasticity, are constructed based on the bulk behavior of many dislocations. Once the FE mesh size approaches the atomic spacing, the possibility of many dislocations becomes impossible, the bulk assumption disappears, and the constitutive relation is invalidated.

Another major problem in multi-scale simulations is that of pathological wave reflection, which occurs at the interface between the MD and FE regions. The issue is that the wavelength emitted by the MD region is considerably smaller than that which can be captured by the continuum FE region. Because of this and the fact that an energy conserving formulation is typically used, the wave must go somewhere and is thus reflected. This leads to spurious heat generation in the MD region, and a contamination of the simulation. One method used by Abraham and Rudd to eliminate this was to mesh the FE region down to the atomic scale so that the FE mesh is small enough that it can represent the short wavelengths emitted from the MD region. Despite this effort, other effects such as stiffness differences between the two regions still cause a small amount of wave reflection.

A small example shows the necessity of accounting for and removing wave reflection. The example problem is that used by Wagner and Liu in their 1D bridging scale paper [9], in which the harmonic potential is used to simulate the atomic interactions. In the bridging scale, as will be discussed in later sections, the MD region constitutes only a small portion of the domain, while the finite element representation is *everywhere* in the domain. The example problem was run with two cases, and the results are shown in Figs. 16 and 17. In the first case, the MD region is directly coupled to the FE region. The resulting wave reflection

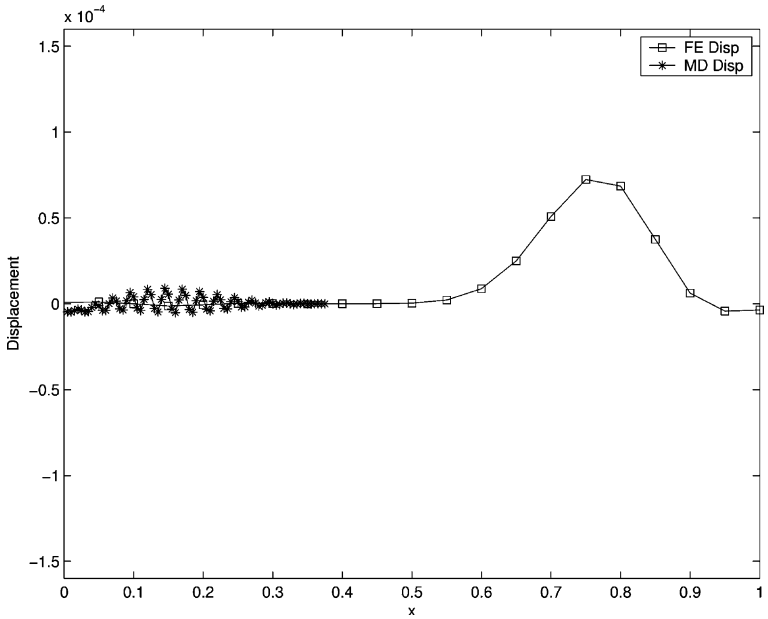

Fig. 16. Depiction of spurious wave reflection which results if MD and FEM regions are directly coupled with no special treatment.

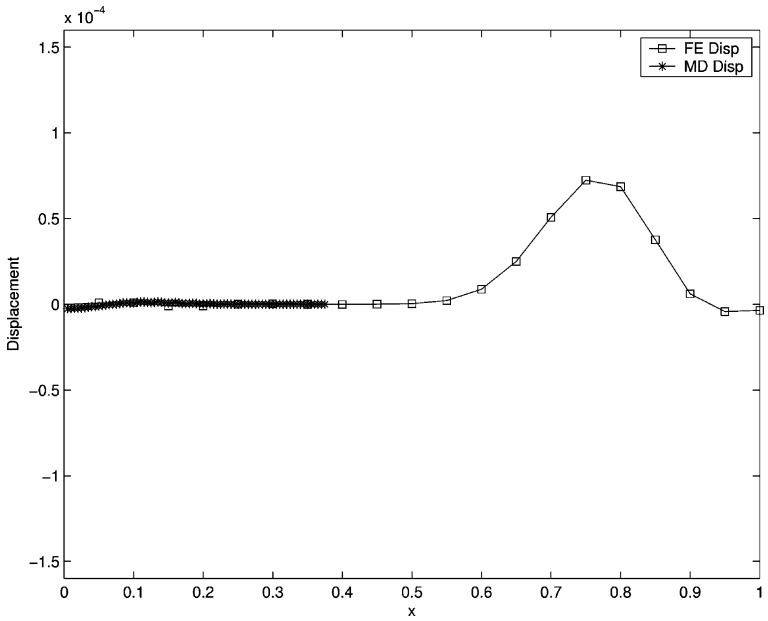

Fig. 17. Removal of spurious wave reflection using GLE.

can clearly be seen in the MD region. In the second example, the boundary physics are correctly accounted for using a technique described below, the generalized Langevin equation (GLE). In comparing the MD displacement after the wave has propagated out of the MD region, it is clear there is almost no reflection in the MD region.

Fig. 18 shows a more quantifiable measure of wave reflection, by measuring the energy remaining in the MD system after the wave has passed through. In this example and for all examples to come in this work regarding energy transfer, the initial energy is the sum of the initial kinetic and potential energy in the MD region, while the final energy is the total kinetic and potential energy remaining in the MD region. If no boundary condition between the MD and FE regions is imposed, it is seen in Fig. 18 that only 30% of the total energy is transferred to the surrounding continuum. However, if the GLE is used, about 99.9% of the total energy is transferred.

1.5. Generalized Langevin equation

Having demonstrated the effect of the GLE in multi-scale simulations, we now qualitatively describe the effect of using this method. Refer to Fig. 19. There, one possible decomposition that develops from using the GLE is shown. Originally, an entire molecular system exists. However, we would like to keep the effects of all the atomistic degrees of freedom while not solving for them explicitly. The reduced MD system that results from using the GLE is then shown. It is shown that the full MD lattice can be reduced into a portion of that lattice along with external forces that act on the boundaries of the reduced lattice which represent the combined effects of all the atomistic degrees of freedom that have been mathematically accounted for. Thus, the GLE can also be used as a boundary condition on an MD simulation; this is the basis for the work in [23,24].

Because the external forces on the reduced lattice are derived from the mathematically accounted for MD degrees of freedom, the effect of using the GLE in conjunction with the FEM is that small wavelengths

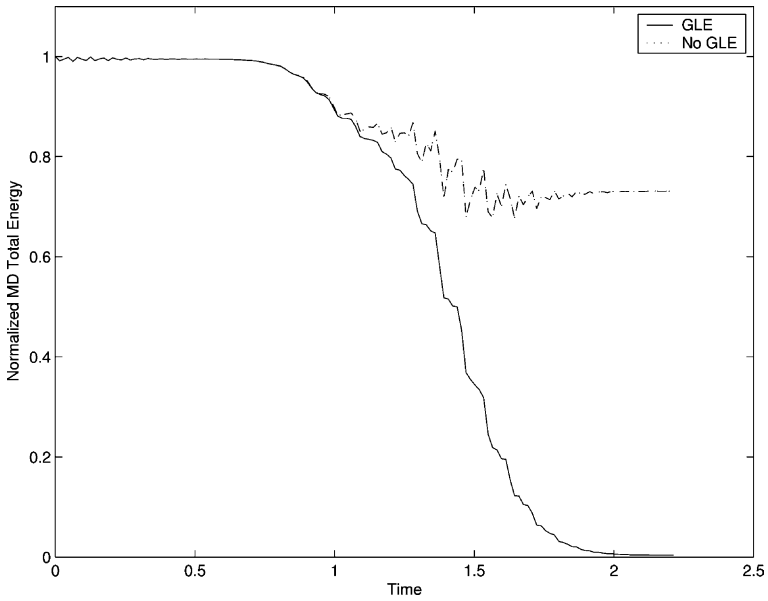

Fig. 18. Energy remaining in MD system using different boundary conditions between MD/FE regions.

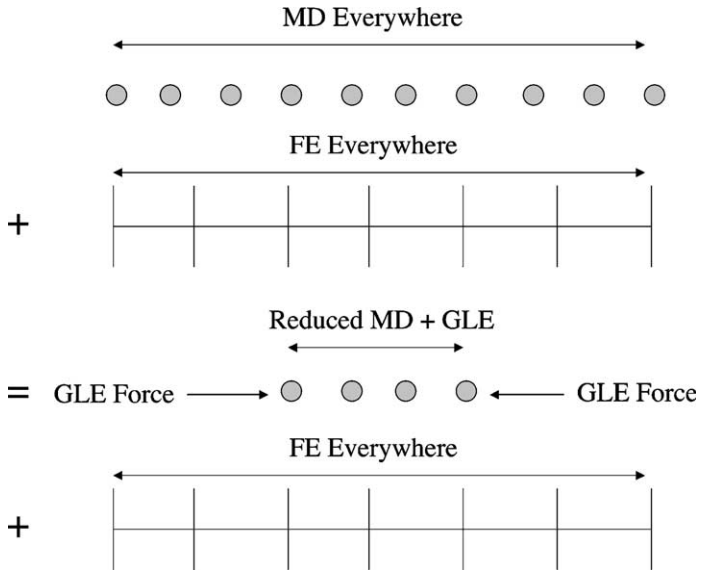

Fig. 19. Schematic of bridging scale method utilizing GLE.

which are on the order of the atomic spacing can be dissipated cleanly into the surrounding continuum, while the FEM can capture any longer wavelength information that is on the order of the FE mesh spacing or larger. The specific details showing the GLE and its relation to the bridging scale will be shown in a later section.

1.5.1. Derivation of generalized Langevin equation

We now derive the GLE as done by Doll and Dion [25] and Adelman and Doll [26]. Assuming a harmonic lattice that vibrates with frequency $\omega = \sqrt{k/m}$, where m is the atomic mass and k is the spring constant, the equations of motion for the atoms can be written in matrix form as

$$\mathbf{M}\ddot{\mathbf{x}}(t) + \mathbf{K}\mathbf{x}(t) = 0. \tag{60}$$

We define region 1 as the MD region where the degrees of freedom will be kept, and region 2 as the MD region to be mathematically accounted for as boundary forces acting on region 1. Decomposing (60) into those parts from regions 1 and 2 and defining $\mathbf{A} = \mathbf{M}^{-1}\mathbf{K}$, the equations of motion are written as

$$\begin{pmatrix} \ddot{\mathbf{x}}_1 \\ \ddot{\mathbf{x}}_2 \end{pmatrix} = -\begin{pmatrix} \mathbf{A}_{11} & \mathbf{A}_{12} \\ \mathbf{A}_{21} & \mathbf{A}_{22} \end{pmatrix} \begin{pmatrix} \mathbf{x}_1 \\ \mathbf{x}_2 \end{pmatrix}. \tag{61}$$

It should be noted that the terms $\mathbf{A}_{12}$ and $\mathbf{A}_{21}$ only play a role near the boundary between regions 1 and 2. For example, if nearest neighbor spring force interactions are considered, then each of those sub-matrices only has one term to account for the interaction of the boundary atom with its nearest neighbors.

The degrees of freedom $\mathbf{x}_2$ are eliminated by solving for them explicitly in (61) and substituting the result back into the equation for $\mathbf{x}_1$. This process is done by Laplace transforming the equation for $\mathbf{x}_2$. In doing so, we briefly review some basic equations related to Laplace transforms. The definition of the Laplace transform of a function $\mathbf{f}(t)$ is

$$\mathbf{F}(s) = \mathscr{L}(\mathbf{f}(t)) = \int_0^\infty \mathbf{f}(t)\,\mathrm{e}^{-st}\,\mathrm{d}t, \tag{62}$$

where the operator $\mathscr{L}$ transforms functions of time t into functions of Laplace space s. The inverse Laplace transform, which transforms functions of Laplace space s into functions of time t is defined to be

$$\mathbf{f}(t) = \mathscr{L}^{-1}(\mathbf{F}(s)) = \frac{1}{2\pi\mathrm{i}} \int_{c-\mathrm{i}\infty}^{c+\mathrm{i}\infty} \mathbf{F}(s)\,\mathrm{e}^{st}\,\mathrm{d}s, \tag{63}$$

where c is a real constant greater than the real parts of all singularities of $\mathbf{F}(s)$. One useful property of Laplace transforms is the convolution property, which states that the convolution integral of two functions is equal to the product of the transforms of the individual functions. Mathematically, this says

$$\mathscr{L}\left(\int_0^t \mathbf{f}(t-t')\mathbf{g}(t')\,\mathrm{d}t' \right) = \mathbf{F}(s)\mathbf{G}(s). \tag{64}$$

A final relevant property of Laplace transforms concerns the transforms of time derivatives. Specifically relevant to this problem is the Laplace transform of a second derivative with respect to time, which can be written as

$$\mathscr{L}\left(\frac{\mathrm{d}^2\mathbf{f}(t)}{\mathrm{d}t^2} \right) = s^2\mathbf{F}(s) - s\mathbf{F}(t=0) - \frac{\mathrm{d}\mathbf{f}}{\mathrm{d}t}(t=0). \tag{65}$$

Using these properties to Laplace transform the equation for $\ddot{\mathbf{x}}_2$ in (61) gives

$$s^2\mathbf{x}_2(s) - s\mathbf{x}_2(0) - \dot{\mathbf{x}}_2(0) = -\mathbf{A}_{21}\mathbf{x}_1(s) - \mathbf{A}_{22}\mathbf{x}_2(s). \tag{66}$$

Solving this equation for $\mathbf{x}_2(s)$ gives

$$\mathbf{x}_2(s) = \boldsymbol{\theta}(s)(s\mathbf{x}_2(0) + \dot{\mathbf{x}}_2(0)) - \boldsymbol{\theta}(s)\mathbf{A}_{21}\mathbf{x}_1(s), \tag{67}$$

where the matrix $\boldsymbol{\theta}(s)$ can be written as

$$\boldsymbol{\theta}(s) = (s^2\mathbf{I} + \mathbf{A}_{22})^{-1}. \tag{68}$$

Performing an inverse Laplace transform on (67) and using the convolution rule, an equation for $\mathbf{x}_2(t)$ can be found as

$$\mathbf{x}_2(t) = -\int_0^t \boldsymbol{\theta}(t-\tau)\mathbf{A}_{21}\mathbf{x}_1(\tau)\,\mathrm{d}\tau + \boldsymbol{\theta}(t)\dot{\mathbf{x}}_2(0) + \dot{\boldsymbol{\theta}}(t)\mathbf{x}_2(0). \tag{69}$$

Substituting (69) into (61) yields an equation for $\ddot{\mathbf{x}}_1(t)$

$$\ddot{\mathbf{x}}_1(t) = -\mathbf{A}_{11}\mathbf{x}_1(t) + \mathbf{A}_{12}\int_0^t \boldsymbol{\theta}(t-\tau)\mathbf{A}_{21}\mathbf{x}_1(\tau)\,\mathrm{d}\tau - \mathbf{A}_{12}\mathbf{x}_2^R(t), \tag{70}$$

where $\mathbf{x}_2^R(t)$ is

$$\mathbf{x}_2^R(t) = \boldsymbol{\theta}(t)\dot{\mathbf{x}}_2(0) + \dot{\boldsymbol{\theta}}(t)\mathbf{x}_2(0). \tag{71}$$

This can now be written in its final form

$$\ddot{\mathbf{x}}_1(t) = -\mathbf{A}_{11}\mathbf{x}_1(t) + \int_0^t \boldsymbol{\Theta}(t-\tau)\mathbf{x}_1(\tau)\,\mathrm{d}\tau + \mathbf{R}(t), \tag{72}$$

where

$$\mathbf{R}(t) = -\mathbf{A}_{12}\mathbf{x}_2^R(t) \tag{73}$$

and

$$\boldsymbol{\Theta}(t) = \mathbf{A}_{12}\boldsymbol{\theta}(t)\mathbf{A}_{21}. \tag{74}$$

As can be seen in (72), the equations of motion for the region 1 atoms have been modified to include two additional terms. These two terms represent the mathematically accounted for degrees of freedom in region 2 in the form of external forces acting upon the boundary atoms of region 1. More specifically, the effects of the mathematically accounted for degrees of freedom in region 2 enter through the time history kernel $\boldsymbol{\Theta}(t)$ and the random force $\mathbf{R}(t)$. It is the time history kernel that mimics the collective behavior of the mathematically accounted for MD degrees of freedom in region 2, and thus is the key element to allowing small wavelengths to pass into the surrounding continuum.

The random force $\mathbf{R}(t)$ captures the exchange of energy between regions 1 and 2 due to temperature differences. The reason this external force is considered random is because this term depends on the initial conditions $\mathbf{x}_2(0)$ and $\dot{\mathbf{x}}_2(0)$, which in general are not known. The initial conditions in region 2 are not known because those degrees of freedom were mathematically eliminated in order to construct the Langevin equation. Furthermore, the temperature T of a solid is in general the only information known, hence the initial conditions can only be determined via a probability distribution. Therefore, a large number of initial conditions are possible, and the force is thus considered random.

Similar approaches have been undertaken by both Cai et al. [27] and E and Huang [28]. In both of these papers, the goal has been to numerically solve for the time history kernel $\boldsymbol{\Theta}$. In the method of E and Huang, the time history kernel is replaced by a truncated discrete summation. Weights are then chosen to minimize wave reflections. The method of Cai and coworkers involves using an MD simulation on a larger domain to characterize the time history kernel for the problem at hand. One issue with both methods is that they may not be transferable, which means that the method may not work for a general lattice structure, and instead work only for those on which they were originally computed. The GLE, in its original form, is also non-transferable. Techniques to resolve this issue are given in [23,24].

2. Overview of bridging scale

2.1. Introduction

The bridging scale [9] was recently developed by Wagner and Liu to couple atomistic and continuum simulations. The fundamental idea is to decompose the total displacement field $\mathbf{u}(\mathbf{x})$ into coarse and fine scales

$$\mathbf{u}(\mathbf{x}) = \bar{\mathbf{u}}(\mathbf{x}) + \mathbf{u}'(\mathbf{x}). \tag{75}$$

This decomposition has been used before in solid mechanics by Hughes et al. in the variational multi-scale method [29]. The coarse scale $\bar{\mathbf{u}}$ is that part of the solution which can be represented by a set of basis functions, i.e. finite element shape functions. The fine scale $\mathbf{u}'$ is defined as the part of the solution whose projection onto the coarse scale is zero.

In order to describe the bridging scale, first imagine that a body in any dimension which is described by N_a atoms. The notation used here will mirror that used by Wagner and Liu [9]. The *total* displacement of an atom α is written as $\mathbf{u}_\alpha$. The coarse scale displacement is a function of the initial positions $\mathbf{X}_\alpha$ of the atoms. It should be noted that the coarse scale would at first glance be thought of as a continuous field, since it can be interpolated between atoms. However, because the fine scale is defined only at atomic positions, the total displacement and thus the coarse scale are discrete functions that are defined only at atomic positions. For consistency, greek indices $(\alpha, \beta, \ldots)$ will define atoms for the remainder of this paper, and uppercase roman indices $(I, J, \ldots)$ will define coarse scale nodes.

The coarse scale is defined to be

$$\bar{\mathbf{u}}(\mathbf{X}_\alpha) = \sum_I N_I^\alpha \mathbf{d}_I. \tag{76}$$

Here, $N_I^\alpha = N_I(\mathbf{X}_\alpha)$ is the shape function of node I evaluated at point $\mathbf{X}_\alpha$, and $\mathbf{d}_I$ is the FE nodal displacement associated with node I.

As discussed above, the fine scale in the bridging scale decomposition is simply that part of the total displacement that the coarse scale cannot represent. Thus, the fine scale will be defined to be the projection of the coarse scale subtracted from the *total* solution $\mathbf{u}_\alpha$. We will select this projection operator to minimize the mass-weighted square of the fine scale, which can be written as

$$\text{Error} = \sum_\alpha m_\alpha \left(\mathbf{u}_\alpha - \sum_I N_I^\alpha \mathbf{w}_I \right)^2, \tag{77}$$

m_α is the atomic mass of an atom α and $\mathbf{w}_I$ are temporary nodal (coarse scale) degrees of freedom. It should be emphasized that (77) is only one of many possible ways to define an error metric. In order to solve for $\mathbf{w}$, the error is minimized with respect to $\mathbf{w}$, yielding the following result:

$$\mathbf{w} = \mathbf{M}^{-1}\mathbf{N}^{\mathrm{T}}\mathbf{M}_{\mathrm{A}}\mathbf{u}, \tag{78}$$

where the coarse scale mass matrix $\mathbf{M}$ is defined as

$$\mathbf{M} = \mathbf{N}^{\mathrm{T}}\mathbf{M}_{\mathrm{A}}\mathbf{N}, \tag{79}$$

$\mathbf{M}_{\mathrm{A}}$ is a diagonal matrix with the atomic masses on the diagonal. The fine scale $\mathbf{u}'$ can thus be written as

$$\mathbf{u}' = \mathbf{u} - \mathbf{N}\mathbf{w} \tag{80}$$

or

$$\mathbf{u}' = \mathbf{u} - \mathbf{P}\mathbf{u}, \tag{81}$$

where the projection matrix $\mathbf{P}$ can be defined to be

$$\mathbf{P} = \mathbf{N}\mathbf{M}^{-1}\mathbf{N}^{\mathrm{T}}\mathbf{M}_{\mathrm{A}}. \tag{82}$$

The total displacement $\mathbf{u}_\alpha$ can thus be written as the sum of the coarse and fine scales as

$$\mathbf{u} = \mathbf{N}\mathbf{d} + \mathbf{u} - \mathbf{P}\mathbf{u}. \tag{83}$$

The final term in the above equation is called the bridging scale. It is the part of the solution that must be removed from the total displacement so that a complete separation of scales is achieved, i.e. the coarse and fine scales are orthogonal to each other. This bridging scale approach was first used by Liu et al. to enrich the finite element method with meshfree shape functions [30]. Wagner and Liu [31] used this approach to consistently apply essential boundary conditions in meshfree simulations. Zhang et al. [32] applied the bridging scale in fluid dynamics simulations. Qian recently used the bridging scale in quasi-static simulations of carbon nanotube buckling [33]. The bridging scale was also used in conjunction with a multi-scale constitutive law to simulate strain localization [34].

Now that the details of the bridging scale have been laid out, some comments are in order. In Eq. (77), the fact that an error measure was defined implies that $\mathbf{u}_\alpha$ is the "exact" solution to the problem. This means that *any* atomistic or molecular-level simulation tool could be used to generate the "exact" solution $\mathbf{u}_\alpha$, i.e. ab initio, quantum molecular dynamics, etc. In our case, the atomistic simulation method we choose to be our "exact" solution is molecular dynamics (MD). After determining that the MD displacements shall be referred to by the variable $\mathbf{q}$, Eq. (77) can be re-written as

$$\text{Error} = \sum_\alpha m_\alpha \left(\mathbf{q}_\alpha - \sum_I N_I^\alpha \mathbf{w}_I \right)^2, \tag{84}$$

where the MD displacements $\mathbf{q}$ now take the place of the total displacements $\mathbf{u}$. The equation for the fine scale $\mathbf{u}'$ can now be re-written as

$$\mathbf{u}' = \mathbf{q} - \mathbf{P}\mathbf{q}. \tag{85}$$

The fine scale is now clearly defined to be the difference between the MD solution and its projection onto a pre-determined coarse scale basis. Finally, the equation for the total displacement $\mathbf{u}$ can be re-written as

$$\mathbf{u} = \mathbf{N}\mathbf{d} + \mathbf{q} - \mathbf{P}\mathbf{q}. \tag{86}$$

We close this section by noting that it can be seen from (84) that the fine scale is simply the mass-weighted least-square error associated with projecting the MD solution onto a finite dimensional basis space. This is particularly useful in quasi-static zero temperature simulations, where atomic vibrations are absent. The fine scale can then be interpreted as a built in error estimator to the quality of the coarse scale approximation.

2.2. Multi-scale equations of motion

The next step in the multi-scale process is to couple the MD and FE equations of motion. This is done by first constructing a Lagrangian $\mathscr{L}$, which is defined to be the kinetic energy minus the potential energy

$$\mathscr{L}(\mathbf{u}, \dot{\mathbf{u}}) = \mathscr{K}(\dot{\mathbf{u}}) - V(\mathbf{u}). \tag{87}$$

Ignoring external forces, (87) can be written as

$$\mathscr{L}(\mathbf{u}, \dot{\mathbf{u}}) = \tfrac{1}{2}\dot{\mathbf{u}}^{\mathrm{T}}\mathbf{M}_{\mathrm{A}}\dot{\mathbf{u}} - U(\mathbf{u}), \tag{88}$$

where the $U(\mathbf{u})$ is the interatomic potential energy. Differentiating the total displacement $\mathbf{u}$ with respect to time gives

$$\dot{\mathbf{u}} = \mathbf{N}\dot{\mathbf{d}} + \mathbf{Q}\dot{\mathbf{q}}, \tag{89}$$

where the complimentary projection operator $\mathbf{Q} \equiv \mathbf{I} - \mathbf{P}$. Substituting (89) into the Lagrangian (88) gives

$$\mathscr{L}(\mathbf{d}, \dot{\mathbf{d}}, \mathbf{q}, \dot{\mathbf{q}}) = \tfrac{1}{2}\dot{\mathbf{d}}^{\mathrm{T}}\mathbf{M}\dot{\mathbf{d}} + \tfrac{1}{2}\dot{\mathbf{q}}^{\mathrm{T}}\mathscr{M}\dot{\mathbf{q}} - U(\mathbf{d}, \mathbf{q}), \tag{90}$$

where the fine scale mass matrix $\mathscr{M}$ is defined to be $\mathscr{M} = \mathbf{Q}^{\mathrm{T}}\mathbf{M}_{\mathrm{A}}$. One elegant feature of (90) is that the total kinetic energy has been decomposed into the sum of the coarse scale kinetic energy plus the fine scale kinetic energy.

The multi-scale equations of motion are obtained from the Lagrangian by following the relations

$$\frac{\mathrm{d}}{\mathrm{d}t}\left(\frac{\partial \mathscr{L}}{\partial \dot{\mathbf{d}}}\right) - \frac{\partial \mathscr{L}}{\partial \mathbf{d}} = 0, \tag{91}$$

$$\frac{\mathrm{d}}{\mathrm{d}t}\left(\frac{\partial \mathscr{L}}{\partial \dot{\mathbf{q}}}\right) - \frac{\partial \mathscr{L}}{\partial \mathbf{q}} = 0. \tag{92}$$

Substituting the Lagrangian (90) into (91) and (92) gives

$$\mathbf{M}\ddot{\mathbf{d}} = -\frac{\partial U(\mathbf{d}, \mathbf{q})}{\partial \mathbf{d}} \tag{93}$$

and

$$\mathscr{M}\ddot{\mathbf{q}} = -\frac{\partial U(\mathbf{d}, \mathbf{q})}{\partial \mathbf{q}}. \tag{94}$$

The two equations (93) and (94) are coupled through the derivative of the potential energy U, which can be expressed as functions of the interatomic force $\mathbf{f}$ as

$$\mathbf{f} = -\frac{\partial U(\mathbf{u})}{\partial \mathbf{u}}. \tag{95}$$

Expanding the right-hand sides of (93) and (94) with a chain rule and using (95) together with (86) gives

$$\mathbf{M}\ddot{\mathbf{d}} = -\frac{\partial U}{\partial \mathbf{u}}\frac{\partial \mathbf{u}}{\partial \mathbf{d}} = \mathbf{N}^{\mathrm{T}}\mathbf{f}, \tag{96}$$

$$\mathscr{M}\ddot{\mathbf{q}} = -\frac{\partial U}{\partial \mathbf{u}}\frac{\partial \mathbf{u}}{\partial \mathbf{q}} = \mathbf{Q}^{\mathrm{T}}\mathbf{f}. \tag{97}$$

Using the fact that $\mathscr{M} = \mathbf{Q}^{\mathrm{T}}\mathbf{M}_{\mathrm{A}}$, (97) can be rewritten as

$$\mathbf{Q}^{\mathrm{T}}\mathbf{M}_{\mathrm{A}}\ddot{\mathbf{q}} = \mathbf{Q}^{\mathrm{T}}\mathbf{f}. \tag{98}$$

Because $\mathbf{Q}$ can be proven to be a singular matrix, there are many unique solutions to (98). However, one solution which does satisfy (98) and is beneficial to us is

$$\mathbf{M}_{\mathrm{A}}\ddot{\mathbf{q}} = \mathbf{f}, \tag{99}$$

$$\mathbf{M}\ddot{\mathbf{d}} = \mathbf{N}^{\mathrm{T}}\mathbf{f}(\mathbf{u}), \tag{100}$$

Eqs. (99) and (100) define the coupled multi-scale equations of motion. As can be seen, (99) is simply the MD equation of motion. Therefore, a standard MD solver can be used to obtain the MD displacements $\mathbf{q}$, while the MD forces $\mathbf{f}$ can be found by minimizing any relevant potential energy function. Furthermore, we can use standard finite element methods to find the solution to (100). One important point is that because

the consistent mass matrix is used to decouple the kinetic energies of the coarse and fine scales, the finite element mass matrix $\mathbf{M}$ must be a consistent mass matrix. It is also crucial to note that while the MD equation of motion is only solved in the MD region, the FE equation of motion is solved *everywhere*.

The coupling between the two equations is through the coarse scale internal force $\mathbf{N}^{\mathrm{T}}\mathbf{f}(\mathbf{u})$, which is a direct function of the MD internal force $\mathbf{f}$. In the region in which MD exists, the coarse scale force is calculated by interpolating the MD force. In the region in which MD has been mathematically accounted for, the coarse scale force can be calculated in multiple ways. Details are provided in a later section.

Two comments are in order here. The first is that the FE equation of motion is redundant for the case in which the MD and FE regions both exist everywhere in the domain, because the FE equation of motion is simply an approximation to the MD equation of motion. We shall remove this redundancy in the next section, when we create coupled MD/FE equations of motion for systems where the MD region is confined to a small portion of the domain.

The other relevant comment concerns the fact that the total solution $\mathbf{u}$ satisfies the same equation of motion as $\mathbf{q}$, i.e.

$$\mathbf{M}_{\mathrm{A}}\ddot{\mathbf{u}} = \mathbf{f}. \tag{101}$$

This result is due to the fact that $\mathbf{q}$ and $\mathbf{u}$ satisfy the same initial conditions, and will be utilized in deriving the boundary conditions on the MD simulation in a later section.

2.3. Langevin equation for bridging scale

We imagine the bridging scale method to be most applicable to problems in which the MD region is confined to a small portion of the domain, while the coarse scale representation exists everywhere. This coupled system is created by reducing the full system in which the MD region and the coarse scale exists everywhere in the domain; see Fig. 19 or 20 for illustrative examples. As was mentioned, one manner in which we can avoid the explicit solution of the many MD degrees of freedom is to utilize the GLE. We now derive the connection between the GLE and the bridging scale.

The derivation is similar to the one presented above by Adelman and Doll, and mimics that given in [9]. Following the argument given in (101), we use the equality of the MD displacements $\mathbf{q}$ and the total displacement $\mathbf{u}$ to decompose the MD equation of motion as

$$\mathbf{M}_{\mathrm{A}}\ddot{\mathbf{q}} = \mathbf{M}_{\mathrm{A}}\ddot{\bar{\mathbf{u}}} + \mathbf{M}_{\mathrm{A}}\ddot{\mathbf{u}}' = \mathbf{f}(\mathbf{u}). \tag{102}$$

The force $\mathbf{f}(\mathbf{u})$ is then Taylor expanded about $\mathbf{u}' = 0$, giving

$$\mathbf{M}_{\mathrm{A}}\ddot{\bar{\mathbf{u}}} + \mathbf{M}_{\mathrm{A}}\ddot{\mathbf{u}}' = \mathbf{f}(\bar{\mathbf{u}}) - \mathbf{K}\mathbf{u}' + \cdots \tag{103}$$

where the stiffness $\mathbf{K}$ is defined as

$$\mathbf{K}_{\alpha\beta} = -\left.\frac{\partial \mathbf{f}_\alpha}{\partial \mathbf{u}_\beta}\right|_{\mathbf{u}'=0}. \tag{104}$$

Three assumptions have been made in the preceding steps:

(1) The Taylor expansion (linearization) of the force in (103) is truncated after linear terms in $\mathbf{u}'$.
(2) Eq. (103) can be decomposed into two separate equations

$$\mathbf{M}_{\mathrm{A}}\ddot{\bar{\mathbf{u}}} = \mathbf{f}(\bar{\mathbf{u}}), \tag{105}$$

$$\mathbf{M}_{\mathrm{A}}\ddot{\mathbf{u}}' = -\mathbf{K}\mathbf{u}'. \tag{106}$$

(3) The stiffness matrix $\mathbf{K}$ is assumed not to vary on short time scales, i.e. the time scale of atomic vibrations.

The three assumptions given above are satisfied if the interatomic potential is harmonic, which means that $\mathbf{K}$ is a constant and the interatomic forces are linear in $\mathbf{u}'$. Another crucial point is that this assumption will be shown to only be necessary at the MD/FE boundary. Continuing with the derivation, the fine scale Eq. (106) is rewritten as

$$\ddot{\mathbf{u}}' = -\mathbf{A}\mathbf{u}', \tag{107}$$

where $\mathbf{A} = \mathbf{M}_{\mathrm{A}}^{-1}\mathbf{K}$. The fine scale degrees of freedom are further partitioned into two vectors: $\mathbf{u}'_1$, the degrees of freedom to be simulated by MD, and $\mathbf{u}'_2$, the degrees of freedom which will be mathematically accounted for in the GLE. Eq. (107) is now written in partitioned matrix form as

$$\begin{pmatrix} \ddot{\mathbf{u}}'_1 \\ \ddot{\mathbf{u}}'_2 \end{pmatrix} = -\begin{pmatrix} \mathbf{A}_{11} & \mathbf{A}_{12} \\ \mathbf{A}_{21} & \mathbf{A}_{22} \end{pmatrix} \begin{pmatrix} \mathbf{u}'_1 \\ \mathbf{u}'_2 \end{pmatrix}. \tag{108}$$

It should be noted that the terms $\mathbf{A}_{12}$ and $\mathbf{A}_{21}$ only play a role near the boundary. For example, if nearest neighbor spring force interactions are considered, then each of those sub-matrices only has one term to account for the interaction of the boundary atom with its nearest neighbors.

The degrees of freedom $\mathbf{u}'_2$ are eliminated by solving for them explicitly in (108) and substituting the result back into the equation for $\mathbf{u}'_1$. This process is done by transforming the equation for $\mathbf{u}'_2$. Doing this gives

$$s^2\mathbf{u}'_2(s) - s\mathbf{u}'_2(0) - \dot{\mathbf{u}}'_2(0) = -\mathbf{A}_{21}\mathbf{u}'_1(s) - \mathbf{A}_{22}\mathbf{u}'_2(s). \tag{109}$$

Rearranging this equation gives

$$\mathbf{u}'_2(s) = -\boldsymbol{\Theta}(s)\mathbf{A}_{21}\mathbf{u}'_1(s) + \boldsymbol{\Theta}(s)(s\mathbf{u}'_2(0) + \dot{\mathbf{u}}'_2(0)), \tag{110}$$

where

$$\boldsymbol{\Theta}(s) = (s^2\mathbf{I} + \mathbf{A}_{22})^{-1}. \tag{111}$$

Taking the inverse Laplace transform of (110) gives the desired expression for $\mathbf{u}'_2(t)$ as

$$\mathbf{u}'_2(t) = -\int_0^t \boldsymbol{\Theta}(t-\tau)\mathbf{A}_{21}\mathbf{u}'_1(\tau)\,\mathrm{d}\tau + \dot{\boldsymbol{\Theta}}(t)\mathbf{u}'_2(0) + \boldsymbol{\Theta}(t)\dot{\mathbf{u}}'_2(0). \tag{112}$$

Substituting this equation into the equation for $\mathbf{u}'_1$ in (108) gives

$$\ddot{\mathbf{u}}'_1(t) = -\mathbf{A}_{11}\mathbf{u}'_1(t) + \int_0^t \boldsymbol{\theta}(t-\tau)\mathbf{u}'_1(\tau)\,\mathrm{d}\tau + \mathbf{R}(t), \tag{113}$$

where $\mathbf{R}(t)$ is

$$\mathbf{R}(t) = -\mathbf{A}_{12}(\dot{\boldsymbol{\Theta}}(t)\mathbf{u}'_2(0) + \boldsymbol{\Theta}(t)\dot{\mathbf{u}}'_2(0)) \tag{114}$$

and

$$\boldsymbol{\theta}(t-\tau) = \mathbf{A}_{12}\boldsymbol{\Theta}(t-\tau)\mathbf{A}_{21}. \tag{115}$$

Recalling that the MD equation of motion can be scale decomposed into coarse and fine scale parts, i.e. (102), we add (113) and (105) to give

$$\ddot{\mathbf{q}}_1(t) = \mathbf{M}_{\mathrm{A}1}^{-1}\mathbf{f}_1(\bar{\mathbf{u}}) - \mathbf{A}_{11}\mathbf{u}'_1(t) + \int_0^t \boldsymbol{\theta}(t-\tau)\mathbf{u}'_1(\tau)\,\mathrm{d}\tau + \mathbf{R}(t). \tag{116}$$

The final step to obtaining the coupled equations is to note that

$$\mathbf{M}_{\mathrm{A1}}^{-1}\mathbf{f}_1(\bar{\mathbf{u}}) - \mathbf{A}_{11}\mathbf{u}_1'(t) = \mathbf{M}_{\mathrm{A1}}^{-1}\mathbf{f}_1(\bar{\mathbf{u}}, \mathbf{u}_1', \mathbf{u}_2' = 0). \tag{117}$$

Substituting (117) into (116) gives

$$\ddot{\mathbf{q}}_1(t) = \mathbf{M}_{\mathrm{A1}}^{-1}\mathbf{f}_1(\bar{\mathbf{u}}, \mathbf{u}_1', \mathbf{u}_2' = 0) + \int_0^t \boldsymbol{\theta}(t-\tau)\mathbf{u}_1'(\tau)\,\mathrm{d}\tau + \mathbf{R}(t). \tag{118}$$

We write the final form of the MD equations of motion by noting that the fine scale component of the MD displacements can be written as

$$\mathbf{u}_1'(\tau) = \mathbf{q}_1(\tau) - \bar{\mathbf{u}}_1(\tau). \tag{119}$$

The final form for the MD equations of motion then becomes

$$\ddot{\mathbf{q}}_1(t) = \mathbf{M}_{\mathrm{A1}}^{-1}\mathbf{f}_1(\bar{\mathbf{u}}, \mathbf{u}_1', \mathbf{u}_2' = 0) + \int_0^t \boldsymbol{\theta}(t-\tau)(\mathbf{q}_1(\tau) - \bar{\mathbf{u}}_1(\tau))\,\mathrm{d}\tau + \mathbf{R}(t). \tag{120}$$

This form for the MD equations of motions differs from that previously presented in [9] in the following manner. Firstly, only displacements and not velocities from the MD and FEM simulations are needed. This allows the usage of the simplest time integration algorithms for both simulations, i.e. velocity verlet and explicit central difference, as will be shown in a later section. The fact that only displacements are present in the time history kernel also lends itself nicely for numerical evaluation of the time history kernel, as explained in [23,24].

The first term on the right-hand side of (120) is simply the interatomic force calculated assuming that the fine scale in region 2 is zero. In simpler terms, this is just the standard interatomic force that is calculated in the MD simulation. Away from the MD boundary, this is the only term that remains from (120), and the standard MD equations of motion result.

The second term on the right-hand side of (120) contains the time history kernel $\boldsymbol{\theta}(t-\tau)$, and acts to dissipate fine scale energy from the MD simulation into the surrounding continuum. The numerical result is a non-reflecting boundary between the MD and FE regions, as the time history kernel allows short wavelengths that cannot be represented by the surrounding continuum to leave the MD region. For a harmonic solid, the time history kernel can be evaluated analytically.

The final term on the right-hand side is the random force $\mathbf{R}(t)$. As was described in a previous section, the random force arises due to temperature differences between the MD region and the surrounding coarse scale. In this work, we assume the random force to be zero, which implies that the temperature of the surrounding continuum is $0K$.

One issue in evaluating (120) is the time history integral involving $\boldsymbol{\theta}(t-\tau)$. In the work by Wagner and Liu, this expression was evaluated in closed form. However, in multiple dimensions and a general lattice structure, a closed form solution may not be possible. Recently, Wagner et al. [24] have developed a means of numerically calculating the time history integral using numerical inverse Laplace transform techniques. The computational effort necessary to pursue such approaches in multiple dimensions, along with the relevant efficiency characteristics, have been explored by Karpov et al. [23] in the context of wave-transmitting boundary conditions for MD simulations.

The main ramification of using a GLE in the bridging scale method is that the atoms in region 2 are mathematically accounted for and act upon the atoms in region 1 through the external forces in (120). These external forces acting upon region 1 are the net resultant of collective behavior of the atoms in region 2. Computationally, this approach virtually eliminates spurious wave reflection between the MD and FE regions, which was one of the key factors mentioned previously in managing an accurate multiple-scale method.

Therefore, the coupled MD/FE equations of motion can be rewritten as

$$\ddot{\mathbf{q}}_1(t) = \mathbf{M}_{A1}^1 \mathbf{f}_1(\bar{\mathbf{u}}, \mathbf{u}_1', \mathbf{u}_2' = 0) + \int_0^t \boldsymbol{\theta}(t-\tau)(\mathbf{q}_1(\tau) - \bar{\mathbf{u}}_1(\tau))\,\mathrm{d}\tau + \mathbf{R}(t), \tag{121}$$

$$\mathbf{M}\ddot{\mathbf{d}} = \mathbf{N}^{\mathrm{T}}\mathbf{f}(\mathbf{u}). \tag{122}$$

As can be seen in (121), the MD equations of motion have been modified such that they depend on the FE displacements at the MD/FE interface. Now, the FE equation of motion is *not* redundant, as the time history integral depends on FE degrees of freedom. The MD degrees of freedom are coupled to the FE equations of motion everywhere, while the FE degrees of freedom affect the MD equations of motion by the terms which act on the boundary atom.

The major advantage of this is that finite-sized domains can be considered with this coupled approach. One example of this is in modeling dynamic crack propagation. If the cracks were modeled using a purely MD system, the major problem is that due to the number of atoms that would be required, the actual problem size cannot be simulated. If the coupled simulation is used, then the waves emitted from the crack tip can naturally propagate away into the far away continuum, such that a realistic problem size can be considered.

Another problem that the bridging scale seems well-suited for is strain localization, as was discussed in the introduction. Because the waves emitting from the localized zone are typically of the elastic variety, the bridging scale boundary conditions derived above should allow the passage of those waves into the surrounding continuum. Furthermore, the evolution of the localized region can be on a smaller time scale than the surrounding continuum, which means that precious computational effort will not be wasted in updating the continuum variables at each timestep with the atomistic variables. Coupling of the bridging scale with a multi-scale material model has been proposed in the work by Kadowaki and Liu [34].

2.3.1. Comments on time history kernel

As was discussed above, one crucial element to the treatment of fine scale waves at the MD/FE boundary is the time history kernel $\boldsymbol{\theta}$. In [9], $\boldsymbol{\theta}$ was derived in 1D assuming a harmonic lattice, and was shown to be

$$\boldsymbol{\theta}(t) = \frac{2k}{t} J_1(2\omega t), \tag{123}$$

where J_1 indicates a first order Bessel function, k is the spring stiffness, and the frequency $\omega = \sqrt{k/m_a}$. The spring stiffness can be determined in general by

$$k = \frac{\partial^2 \Phi(\mathbf{r})}{\partial \mathbf{r}^2}. \tag{124}$$

For a harmonic solid, k is simply the spring stiffness. For the Lennard-Jones examples to be presented in a later section, the following definition will be used for k:

$$k = \frac{624\epsilon}{\sigma^2 y^{14}} - \frac{168\epsilon}{\sigma^2 y^8}, \tag{125}$$

where $y = 2^{1/6}$.

2.3.2. Comparison between bridging scale and existing multi-scale methods

Now that the development of the bridging scale theory has been completed, a comparison between the bridging scale and the other multi-scale methods is in order. The first point of comparison stems from the

fact that the bridging scale is an approach inherently geared for dynamics problems. While it can be easily applied to static problems (see for example Qian et al. [35]), the current applications have been in dynamic simulations. This lies in comparison to the quasi-continuum method, which to date has been used only for quasi-static problems.

In comparing the bridging scale to the other dynamic multi-scale methods (CGMD, MAAD), one clear advantage for the bridging scale is that the coarse scale is represented everywhere, and is *not* meshed down to the atomic scale. The effect of this is that the coarse scale timestep is not restricted by the smallest, atomic-sized elements in the mesh. More importantly, this allows the use of a staggered time integration scheme, as was detailed by Wagner and Liu [9]. Thus, the coarse scale variables can evolve on an appropriate time scale, while the fine scale variables can evolve (appropriately) on a much smaller time scale.

A final advantage of the bridging scale is that no ad hoc treatment is needed to couple the MD and FE regions at the MD/FE boundary. Instead, the MD lattice behaves as if part of a larger lattice due to the GLE, which allows the high frequency information typically found in the MD region to naturally dissipate into the continuum. Furthermore, the GLE is a mathematically exact representation of the MD degrees of freedom which are not explicitly solved for. Finally, the FE simulation provides part of the boundary force on the MD simulation through the additional terms present in the modified MD equation of motion.

2.3.3. Cauchy–Born rule for coarse scale

In the coarse scale, where the MD force is unavailable (i.e. region 2 in Fig. 20), an approximation to the right-hand side of (122), the $\mathbf{N}^{\mathrm{T}}\mathbf{f}$ term, must be made. The goal is to utilize the MD potential in the expression for the coarse scale force. The Cauchy–Born rule is one way to accomplish this. First, we assume that the potential energy $U(\mathbf{u})$ for the system can be decomposed as

$$U(\mathbf{u}) = \sum_{\alpha} W_{\alpha}(\mathbf{u})\,\Delta V_{\alpha}, \tag{126}$$

where W_{α} is the potential energy *density* centered at atom α. Comparing the right-hand sides of (93) and (96), we find the relation

$$(\mathbf{N}^{\mathrm{T}}\mathbf{f})_I = -\frac{\partial U(\mathbf{u})}{\partial \mathbf{d}_I}. \tag{127}$$

Substituting (126) into (127), we obtain

$$(\mathbf{N}^{\mathrm{T}}\mathbf{f})_I = -\sum_{\alpha} \frac{\partial W_{\alpha}(\mathbf{u})}{\partial \mathbf{d}_I}\Delta V_{\alpha}. \tag{128}$$

In order to use the Cauchy–Born rule, we use a chain rule on (128) to obtain

$$(\mathbf{N}^{\mathrm{T}}\mathbf{f})_I = -\sum_{\alpha} \frac{\partial W_{\alpha}}{\partial \mathbf{F}_{\alpha}^{\mathrm{T}}}\frac{\partial \mathbf{F}_{\alpha}^{\mathrm{T}}}{\partial \mathbf{d}_I}\Delta V_{\alpha}. \tag{129}$$

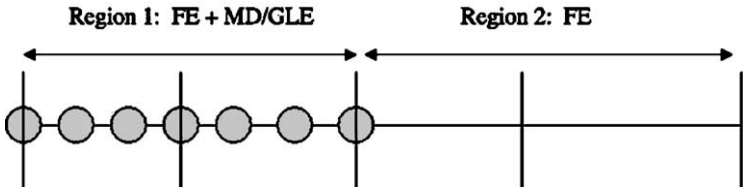

Fig. 20. Separation of problem into two regions. Region 1 is FE + reduced MD, region 2 is FE.

Simplifying further,

$$(\mathbf{N}^{\mathrm{T}}\mathbf{f})_I = -\sum_{\alpha} \frac{\partial N_I}{\partial \mathbf{X}}\bigg|_{\mathbf{X}=\mathbf{X}_\alpha} \frac{\partial W_\alpha}{\partial \mathbf{F}_\alpha^{\mathrm{T}}} \Delta V_\alpha. \tag{130}$$

Noting that the derivative of the energy density W with respect to $\mathbf{F}^{\mathrm{T}}$ gives the first Piola–Kirchoff stress $\mathscr{P}$, the summation in (130) can be approximated by a discrete summation as

$$(\mathbf{N}^{\mathrm{T}}\mathbf{f})_I = -\sum_{q} \frac{\partial N_I}{\partial \mathbf{X}}(\mathbf{X}_q)\mathscr{P}(\mathbf{X}_q) w_q, \tag{131}$$

where w_q is the integration weight associated with point $\mathbf{X}_q$.

2.3.4. Direct application of MD potential for coarse scale

An alternative approach was adopted by Qian et al. [35]. In order to utilize realistic potentials, Qian noted that the potential energy $\Phi(\mathbf{u})$ is a function of the total displacement $\mathbf{u}$. However, most potential energy expressions are functions of the distance $\mathbf{r}_{\alpha\beta}$ between two atoms α and β. In order to do so, we first write the distance $\mathbf{r}_{\alpha\beta}$ as a function of $\mathbf{u}$ as

$$\mathbf{r}_{\alpha\beta} = \mathbf{X}_{\alpha\beta} + \mathbf{u}_{\alpha\beta}, \tag{132}$$

where $\mathbf{r}_{\alpha\beta} = \mathbf{r}_\alpha - \mathbf{r}_\beta$ and $\mathbf{X}_{\alpha\beta}$ are the initial positions of the atoms. By using the finite element approximation of the total displacement, we can rewrite (132) as

$$\mathbf{r}_{\alpha\beta} = \mathbf{X}_{\alpha\beta} + \sum_I (N_I(\mathbf{X}_\alpha) - N_I(\mathbf{X}_\beta))\mathbf{d}_I. \tag{133}$$

Taking the derivative of (133) gives

$$\frac{\partial \mathbf{r}_{\alpha\beta}}{\partial \mathbf{d}_I} = \sum_I (N_I(\mathbf{X}_\alpha) - N_I(\mathbf{X}_\beta)). \tag{134}$$

We assume that the potential energy for the system can be decomposed into the sum of the potential energies in each bond as

$$U(\mathbf{u}) = \sum_{\alpha} \Phi_\alpha. \tag{135}$$

Taking a chain rule derivative on the right-hand side of (135) gives

$$(\mathbf{N}^{\mathrm{T}}\mathbf{f})_I = -\frac{\partial U(\mathbf{u})}{\partial \mathbf{d}_I} = -\sum_{\alpha}\sum_{\alpha\neq\beta} \frac{\partial \Phi_\alpha(\mathbf{r}_{\alpha\beta})}{\partial \mathbf{r}_{\alpha\beta}} \frac{\partial \mathbf{r}_{\alpha\beta}}{\partial \mathbf{d}_I} \Delta V_\alpha. \tag{136}$$

The additional summation $\alpha \neq \beta$ enters because minimizing the energy requires a loop over all atoms excluding the atom under consideration. Substituting in (134) gives the final expression for the coarse scale force

$$(\mathbf{N}^{\mathrm{T}}\mathbf{f})_I = -\sum_{\alpha}\sum_{\alpha\neq\beta} \frac{\partial \Phi_\alpha(\mathbf{r}_{\alpha\beta})}{\partial \mathbf{r}_{\alpha\beta}} \sum_I (N_I(\mathbf{X}_\alpha) - N_I(\mathbf{X}_\beta))\Delta V_\alpha. \tag{137}$$

The next step is to evaluate this expression only at discrete points in the coarse scale, or the quadrature points. Denoting the reduced set of atomic positions as $\bar{\alpha}$, we rewrite (137) in discrete form as

$$(\mathbf{N}^{\mathrm{T}}\mathbf{f})_I \approx -\sum_{\bar{\alpha}}\sum_{\bar{\alpha}\neq\bar{\beta}} w_{\bar{\alpha}} \frac{\partial \Phi_{\bar{\alpha}}(\mathbf{r}_{\bar{\alpha}\bar{\beta}})}{\partial \mathbf{r}_{\bar{\alpha}\bar{\beta}}} \sum_I (N_I(\mathbf{X}_{\bar{\alpha}}) - N_I(\mathbf{X}_{\bar{\beta}})), \tag{138}$$

where $w_{\tilde{\alpha}}$ is the integration weight associated with quadrature point $\mathbf{X}_{\tilde{\alpha}}$, which replaces the volume term ΔV_α. For comparison, we also restate the final Cauchy–Born equation for the coarse scale

$$(\mathbf{N}^{\mathrm{T}}\mathbf{f})_I = -\sum_q \frac{\partial N_I}{\partial \mathbf{X}}(\mathbf{X}_q)\mathscr{P}(\mathbf{X}_q)w_q. \tag{139}$$

Both of these approaches are based on the philosophy that the coarse scale force should be derived from the same interatomic potential as is used in the MD region. The Cauchy–Born rule is an indirect application of this theory, as the potential energy density is first written in terms of the continuum deformation gradient $\mathbf{F}$. In contrast, the approach adopted by Qian et al. directly applies the MD potential at each coarse scale quadrature point. For the examples in this work, the Cauchy–Born rule was applied to calculate the internal force in the coarse scale.

2.4. Staggered time integration algorithm

As was previously mentioned, one strength of the bridging scale lies in the ability to update the MD and FE equations of motion using appropriate time increments for each equation. In fact, both simulations are integrated through time using widely utilized integration algorithms; velocity verlet for MD, and explicit central difference for FE.

2.4.1. MD update

The basic idea is that for each computational period, both simulations are advanced by a timestep Δt. The MD simulation is advanced first by m steps of size $\Delta t/m$ while the FE simulation is advanced through a single timestep of size Δt. A small modification in the standard MD velocity verlet update is required because the MD simulation requires information from the FE simulation near the boundary (see (121)). The modification is that the FE boundary displacement and velocity will be interpolated at fractional timesteps, while the FE boundary acceleration will be assumed to be constant during the MD time sub-cycle. The FE boundary acceleration is assumed to be constant such that the actual FE equations of motion are not solved at each MD timestep. The stability of similar staggered time integration methods with sub-cycling was explored in [36,37].

Superscripts will be used to denote the timestep, bracket notation $[j]$ will be shorthand for the fractional timestep $n+\frac{j}{m}$, and the sub-cycle timestep will be denoted $\Delta t_m = \Delta t/m$. The subscript Γ will denote FE quantities that are only needed close to the boundary. Finally, $\mathbf{f}(\mathbf{q},\bar{\mathbf{u}},\mathbf{h})$ will represent the entire right-hand size of (121) where $\mathbf{h}$ is used to represent the time history quantities that are needed in the integration. Assuming that $\bar{\mathbf{u}}_\Gamma^n$, $\dot{\bar{\mathbf{u}}}_\Gamma^n$, $\ddot{\bar{\mathbf{u}}}_\Gamma^n$, $\mathbf{q}^n$, $\mathbf{p}^n$ and $\mathbf{s}^n$ are known, these quantities are updated via the velocity verlet algorithm as follows:

$$\bar{\mathbf{u}}_\Gamma^{[j+1]} = \bar{\mathbf{u}}_\Gamma^{[j]} + \dot{\bar{\mathbf{u}}}_\Gamma^{[j]}\,\Delta t_m + \tfrac{1}{2}\ddot{\bar{\mathbf{u}}}_\Gamma^n\,\Delta t_m^2, \tag{140}$$

$$\dot{\bar{\mathbf{u}}}_\Gamma^{[j+1]} = \dot{\bar{\mathbf{u}}}_\Gamma^{[j]} + \ddot{\bar{\mathbf{u}}}_\Gamma^n\,\Delta t_m, \tag{141}$$

$$\mathbf{q}^{[j+1]} = \mathbf{q}^{[j]} + \mathbf{p}^{[j]}\,\Delta t_m + \tfrac{1}{2}\mathbf{s}^{[j]}\,\Delta t_m^2, \tag{142}$$

$$\mathbf{p}^{\left[j+\frac{1}{2}\right]} = \mathbf{p}^{[j]} + \mathbf{s}^{[j]}\,\Delta t_m, \tag{143}$$

$$\mathbf{s}^{[j+1]} = \mathbf{M}_{\mathrm{A}}^{-1}\mathbf{f}(\mathbf{q}^{[j+1]}, \bar{\mathbf{u}}_\Gamma^{[j+1]}, \mathbf{h}^{[j+1]}), \tag{144}$$

$$\mathbf{p}^{[j+1]} = \mathbf{p}^{\left[j+\frac{1}{2}\right]} + \tfrac{1}{2}(\mathbf{s}^{[j+1]} + \mathbf{s}^{[j]})\,\Delta t_m, \tag{145}$$

$\mathbf{p}$ is the MD velocity, $\bar{\mathbf{u}}_{\Gamma}$ is the FE boundary displacement, $\dot{\bar{\mathbf{u}}}_{\Gamma}$ is the FE boundary velocity, $\mathbf{q}$ is the MD displacement, $\mathbf{s}$ is the MD acceleration and $\mathbf{M}_{\mathrm{A}}$ is the MD mass matrix.

2.4.2. FE update

Once the MD quantities are obtained using the above algorithm at time $n+1$, the FE displacements $\mathbf{d}$, velocities $\mathbf{v}$ and accelerations $\mathbf{a}$ are updated from time n to $n+1$. This is done using a central difference scheme:

$$\mathbf{d}^{n+1} = \mathbf{d}^{n} + \mathbf{v}^{n}\,\Delta t + \tfrac{1}{2}\mathbf{a}^{n}\,\Delta t^{2}, \tag{146}$$

$$\mathbf{a}^{n+1} = \mathbf{M}^{-1}\mathbf{N}^{\mathrm{T}}\mathbf{f}(\mathbf{N}\mathbf{d}^{n+1} + \mathbf{Q}\mathbf{q}^{n+1}), \tag{147}$$

$$\mathbf{v}^{n+1} = \mathbf{v}^{n} + \tfrac{1}{2}(\mathbf{a}^{n} + \mathbf{a}^{n+1})\,\Delta t, \tag{148}$$

where $\mathbf{M}$ is the consistent FE mass matrix. The internal force $\mathbf{f}$ is computed by combining the coarse scale part of the displacement $\mathbf{N}\mathbf{d}$ with the fine scale part of the MD simulation $\mathbf{Q}\mathbf{q}$.

3. Bridging scale numerical examples

3.1. Lennard-Jones numerical examples

Due to the fact that the verification of the bridging scale for linear problems was given in [9], the numerical examples here utilize the Lennard-Jones 6-12 potential. For simplicity, σ and ϵ were assumed to be unity, and the atoms were given a prescribed displacement similar to the gaussian wave boundary condition used by Wagner and Liu [9]. Thirty finite elements spanned the entire domain between $x = -150r_0$ and $150r_0$, and 111 atoms were used between $x = -55r_0$ and $55r_0$. The initial amplitude of the wave was 13% of the equilibrium spacing, and the FE nodal spacing was 10 times the MD atomic spacing. Fifty-five FE timesteps were used, with 50 MD timesteps per FE timestep. The FE nodal forces in the coarse scale outside the coupled MD/FE region were calculated using the Cauchy–Born rule using the LJ 6-12 potential. Finally, the random force $\mathbf{R}(t)$ in (121) was taken to be zero, implying that the MD calculation was done at $0K$.

Figs. 21 and 22 show two snapshots of the bridging scale simulation. In comparing the two snapshots, it is clear that the majority of the high frequency (fine scale) component of the MD displacement has been dissipated cleanly into the surrounding continuum. The comparison between the bridging scale energy transfer and the actual MD energy transfer is shown in Fig. 23. It is shown that the bridging scale energy transfer is about 99% of the full MD energy transfer.

3.2. Truncation of time history kernel

An issue that will be crucial in multiple dimensions will be truncating the time history kernel to a computationally manageable size. Recall from (120) that the time history kernel (thk) force is written as

$$\mathbf{f}_{\mathrm{thk}} = \int_{0}^{t} \boldsymbol{\theta}(t-\tau)(\mathbf{q}-\bar{\mathbf{u}})(\tau)\,\mathrm{d}\tau. \tag{149}$$

In order to evaluate this integral exactly, it is necessary to store the displacements of the boundary atoms (and the coarse scale at the MD boundary) for the entire duration of the simulation. In one dimension, this is feasible due to the fact that the time history kernel $\boldsymbol{\theta}$ is known analytically, and furthermore because displacement histories are only necessary for two boundary atoms. In two and three dimensions, because

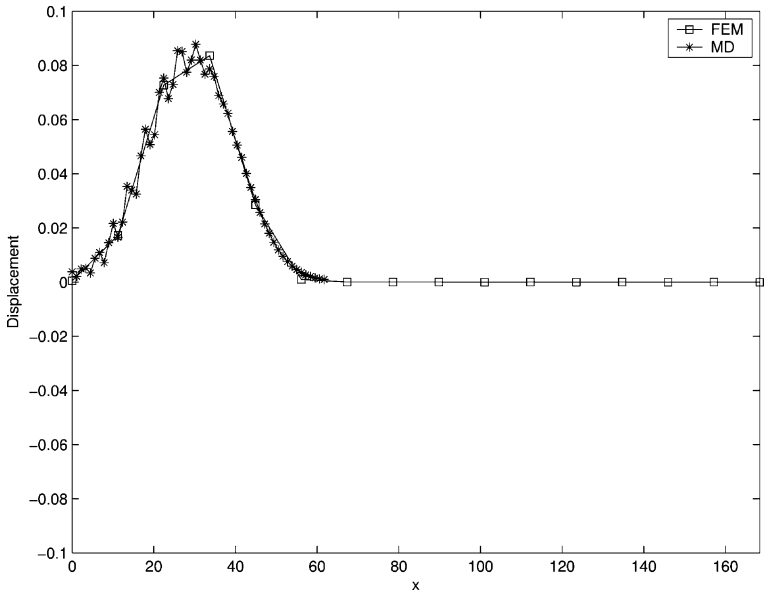

Fig. 21. Snapshot of MD/FE displacements showing fine scale MD displacement component.

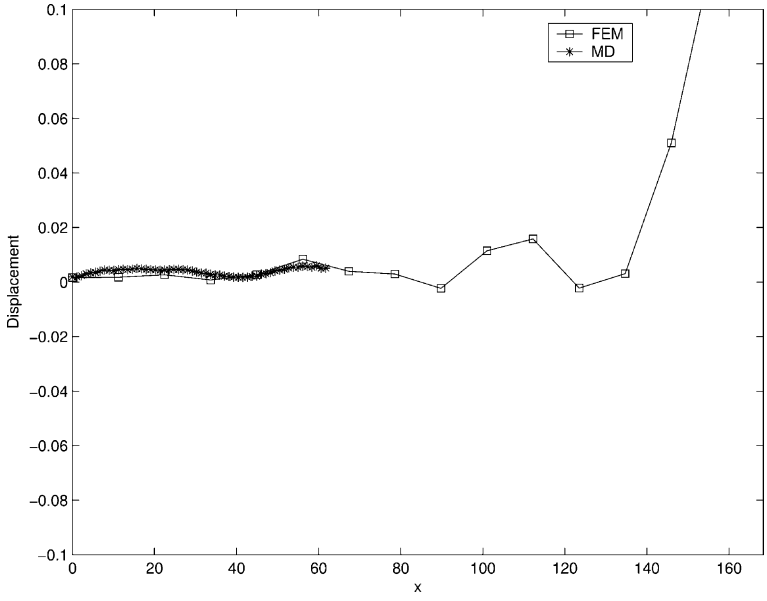

Fig. 22. Snapshot showing majority of fine scale MD information has passed through to coarse scale.

there will be many boundary atoms, any successful approach demands that only a few displacement histories be stored for each boundary atom lest the memory requirements overwhelm the simulation.

Motivated by this fact, we now present a study of time history truncation in one dimension. The basis for the truncation was presented by Karpov et al. [23]. The truncation itself occurs in two forms. The first form

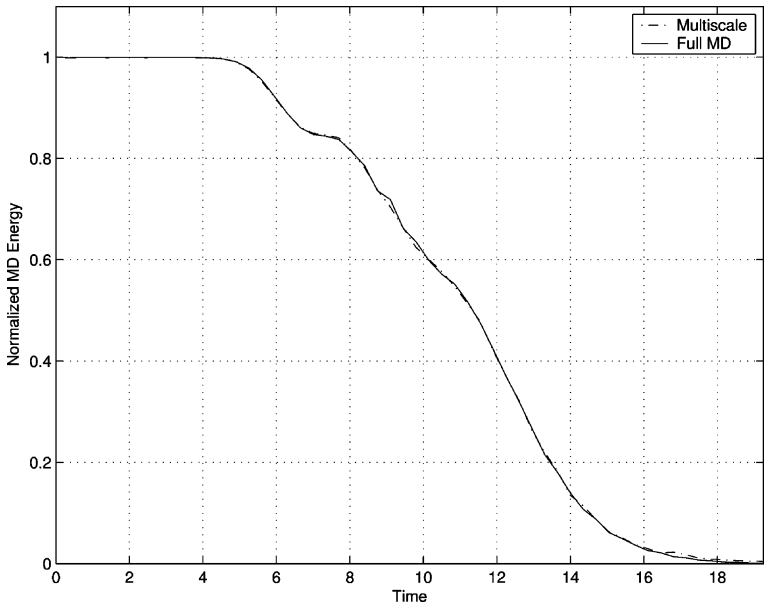

Fig. 23. Bridging scale vs. full MD energy comparison for high frequency displacement initial condition.

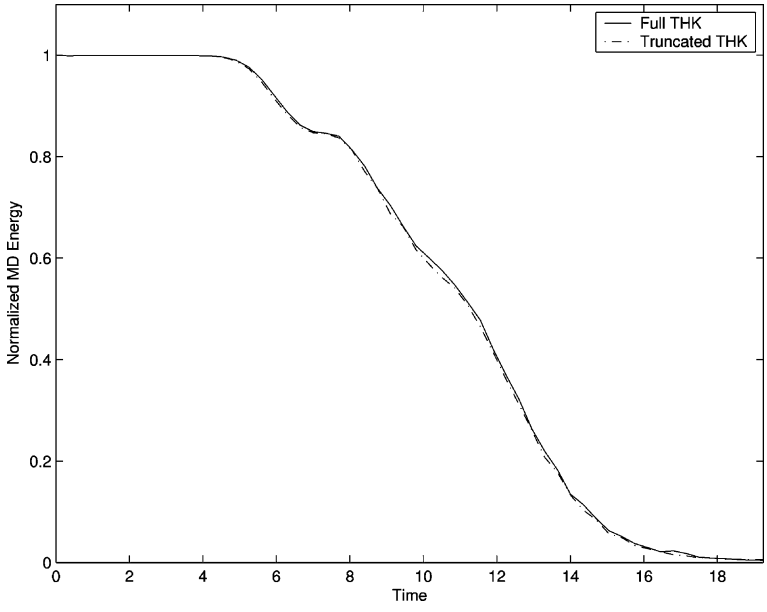

Fig. 24. Comparison between fully integrated time history integral and truncated time history integral.

is motivated by the physical behavior of the time history kernel $\boldsymbol{\theta}$. In Fig. 25, $\boldsymbol{\theta}$ is shown. A salient feature of $\boldsymbol{\theta}$ is that its wave amplitude decreases quickly (to less than 10% of its maximum amplitude) after only a few oscillations. Based on this fact, an approximation is made in which the later components of $\boldsymbol{\theta}$ are deemed to

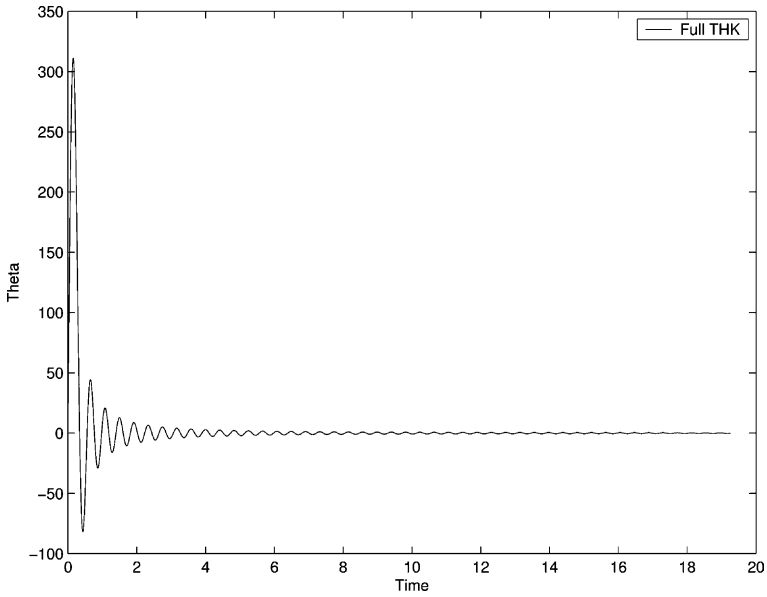

Fig. 25. Plot of time history kernel $\boldsymbol{\theta}$.

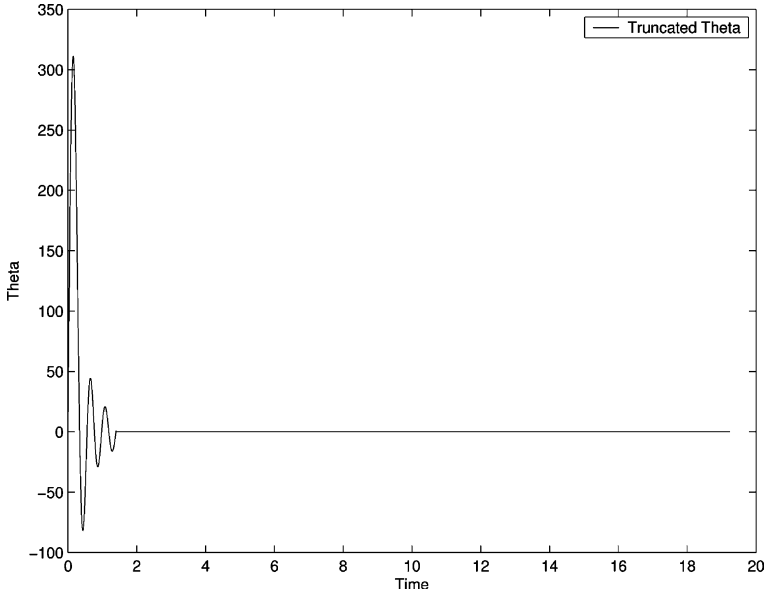

Fig. 26. Plot of time history kernel $\boldsymbol{\theta}$ truncated after three complete oscillations.

be insignificant, and are simply set to zero. This truncation is shown in Fig. 26, where $\boldsymbol{\theta}$ is truncated after three full oscillations.

The second major truncation occurs in the evaluation of the convolution integral (149). By increasing the timestep of the of the convolution integral with respect to the MD simulation timestep, a further significant

computational reduction will occur due to the fact that many fewer boundary atom displacements will need to be stored. If a larger convolution integral timestep is used, the integral in (149) can be re-written as a summation as

$$\mathbf{f}(t_n) = h\,\Delta t \sum_{k=0}^{n,h} \boldsymbol{\theta}_{t_n-\tau_k}(\mathbf{q} - \bar{\mathbf{u}})_{\tau_k}, \tag{150}$$

where t_n is the current time, h is an integer which describes the frequency of the sampling and Δt is the MD timestep. The summation is therefore a discrete summation, with k incremented in factors of h. Therefore, $\mathbf{u}$ does not change in between discrete sampling points, and is only augmented at each discrete sampling point. The factor $h = \frac{\Delta t_{\text{conv}}}{\Delta t_{\text{md}}}$ acts as a quadrature weight which accounts for the remainder of the time history points and displacements which are not stored and hence are not calculated. It is because of this integration weight h that the boundary atom displacement history can be truncated after a small number of points.

The example shown in Fig. 24 shows a comparison between using the fully integrated time history integral and the truncated time history integral using the process just described. The example problem run was the same as the high frequency initial displacement example shown in the previous section using the Lennard-Jones potential. For the truncated time history integral, the truncated $\boldsymbol{\theta}$ shown in Fig. 26 was used. In our simulation, that $\boldsymbol{\theta}$ corresponds to 200 MD timesteps. The boundary atom displacement history was updated every 25 MD timesteps, which means that only 8 displacement histories need to be stored for each boundary atom. This implies that k in (150) has a maximum value of $8h$, and also that $h = 25$.

As can be seen in Fig. 24, the results using the truncated time history kernel are nearly identical to that using the full time history kernel, validating the truncation method proposed. Furthermore, the computational savings is immense; in the full time history integral, the storage of approximately 2700 displacements (i.e. the total number of MD timesteps) is necessary per boundary atom. Moreover, the 2700 is an arbitrary number; the number of displacements stored is simply equal to the total number of timesteps of the MD simulation, which can be much larger. Most importantly, we have established a framework by which the truncation of the time history kernel in multiple dimensions can be easily performed.

4. Conclusions and future research

We have presented a detailed overview of the multiple-scale methods whose goal is to couple atomistic simulations to continuum simulations. The methods discussed herein all have inherent strengths and weaknesses. MAAD has been successfully applied to dynamic fracture simulations. However, the issue of disparate time scales has not been resolved in this approach, as all equations of motion are integrated forward using the same timestep. Furthermore, no special treatment has been used to eliminate wave reflection at the FE/MD interface. The quasi-continuum method has been used to simulate nanoindentation and dislocation generation. However, no extension of the method to dynamic problems has been proposed.

In contrast, the bridging scale method is inherently geared for dynamic problems. The fact that the coarse scale exists everywhere and is not meshed down to the atomic spacing allows for a staggered time integration algorithm, which allows the atomistic and continuum simulations to evolve on their natural time scales. The boundary coupling between the simulations is achieved by use of the Langevin equation, which eliminates fine scale reflection at the interface. Furthermore, the method works naturally for quasi-static problems, as was demonstrated by Qian et al. [35].

The application of the bridging scale to fully non-linear problems in 1D has been shown through example problems. It was demonstrated that the energy transfer from MD to continuum is excellent even for an FE mesh that is coarse compared to the lattice spacing. Even for highly non-linear problems, the

coarse scale (FE) is able to capture the longer wavelengths of the solution, while the use of the time history kernel allows the dissipation of small wavelengths into the continuum. An example was done in which the time history integral was truncated both spatially and temporally for a fully non-linear problem. It was demonstrated that this truncation did not degrade the accuracy of the method, while greatly enhancing the computational efficiency.

The major future thrust of research regarding the bridging scale will be an extension to multiple dimensions. In a generalized multi-dimensional case, the following issues will dominate. Firstly, the issue of memory arises due to the necessity of storing many displacement histories for each MD boundary atom. However, the truncation techniques presented here and in [23] reduce the storage requirements to approximately ten or fifteen previous displacements per boundary atom while not sacrificing accuracy, which makes the memory issue manageable. Another issue that will arise will be the numerical calculation of the time history kernel in multiple dimensions. However, recent work by Karpov et al. [23] and Wagner et al. [24] presents a consistent numerical technique to calculate the time history kernel for a given lattice structure as a function of the parameters of a given interatomic potential. Finally, while the boundary condition for the MD/FE interface was derived for a harmonic lattice, we have shown the accuracy of the method in the case of a large, non-linear perturbation.

Acknowledgements

We would like to thank the National Science Foundation (NSF) and the NSF-IGERT program for their support. We would further like to thank the NSF Summer Institute on Nano Mechanics and Materials. We would also like to extend special thanks to Prof. Dong Qian and Dr. Gregory Wagner for their time and assistance in answering the numerous questions of the authors, and also to Dr. Wagner for developing much of the code which was used for this article. Thanks go to Dr. Shaoping Xiao and Dr. Eduard Karpov for critically reading the manuscript, and also to Dr. Karpov for helpful discussions on the nuances of the time history kernel. Finally, we would like to acknowledge enlightening discussions with Dr. Marino Arroyo on the Cauchy–Born rule.

References

[1] W.K. Liu, E.G. Karpov, S. Zhang, H.S. Park, An introduction to computational nano mechanics and materials, Comput. Methods Appl. Mech. Engrg., in this issue.
[2] M. Zhou, A.J. Rosakis, G. Ravichandran, Dynamically propagating shearbands in impact-loaded prenotched plates—i. experimental investigations of temperature signatures and propagation speed, J. Mech. Phys. Solids 44 (1996) 981–1006.
[3] S. Li, W.K. Liu, A.J. Rosakis, T. Belytschko, W. Hao, Meshfree galerkin simulations of dynamic shearband propagation and failure mode transition, Int. J. Solids Struct. 39 (2002) 1213–1240.
[4] W.K. Liu, S. Jun, Y.F. Zhang, Reproducing kernel particle methods, Int. J. Numer. Methods Fluids 20 (1995) 1081–1106.
[5] W.K. Liu, S. Jun, S. Li, J. Adee, T. Belytschko, Reproducing kernel particle methods for structural dynamics, Int. J. Numer. Methods Engrg. 38 (1995) 1655–1680.
[6] W.K. Liu, Y. Chen, Wavelet and multiple scale reproducing kernel methods, Int. J. Numer. Methods Engrg. 21 (1995) 901–931.
[7] P.R. Guduru, A.J. Rosakis, G. Ravichandran, Dynamic shearbands: an investigation using high speed optical and infrared diagnostics, Mech. Mater. 33 (2001) 371–402.
[8] H.S. Park, MS Thesis, Northwestern University.
[9] G.J. Wagner, W.K. Liu, Coupling of atomistic and continuum simulations using a bridging scale decomposition, Comput. Methods Appl. Mech. Engrg., in press.
[10] F.F. Abraham, J. Broughton, N. Bernstein, E. Kaxiras, Spanning the continuum to quantum length scales in a dynamic simulation of brittle fracture, Europhys. Lett. 44 (1998) 783–787.
[11] J.Q. Broughton, F.F. Abraham, N. Bernstein, E. Kaxiras, Concurrent coupling of length scales: methodology and applications, Phys. Rev. B 60 (1999) 2391–2403.

[12] W.M.C. Foulkes, R. Haydock, Phys. Rev. B 39 (1989) 12520.
[13] F.F. Abraham, J.Q. Broughton, N. Bernstein, E. Kaxiras, Spanning the length scales in dynamic simulation, Comput. Phys. 12 (1998) 538–546.
[14] R.E. Rudd, J.Q. Broughton, Coarse-grained molecular dynamics and the atomic limit of finite elements, Phys. Rev. B 58 (1998) 5893–5896.
[15] W.L.T. Belytschko, B. Moran, Nonlinear Finite Elements for Continua and Structures, John Wiley and Sons, 2002.
[16] R.D. Ruth, IEEE Trans. Nucl. Sci. (1983) 2669.
[17] E. Tadmor, M. Ortiz, R. Phillips, Quasicontinuum analysis of defects in solids, Philos. Mag. A 73 (1996) 1529–1563.
[18] E. Tadmor, R. Phillips, M. Ortiz, Mixed atomistic and continuum models of deformations in solids, J. ACM (1996) 4529–4534.
[19] M. Arroyo, T. Belytschko, An atomistic-based finite deformation membrane for single layer crystalline films, J. Mech. Phys. Solids 50 (2002) 1941–1977.
[20] P. Zhang, Y. Huang, H. Gao, K.C. Hwang, Fracture nucleation in single-wall carbon nanotubes under tension: a continuum analysis incorporating interatomic potentials, J. Appl. Mech. 69 (2002) 454–458.
[21] D.J. Diestler, Coarse-grained descriptions of multiple scale processes in solid systems, Phys. Rev. B 66 (2002) 184104-1–184104-7.
[22] L.E. Shilkrot, W.A. Curtin, R.E. Miller, A coupled atomistic/continuum model of defects in solids, J. Mech. Phys. Solids 50 (2002) 2085–2106.
[23] E.G. Karpov, G.J. Wagner, W.K. Liu, A green's function approach to deriving wave-transmitting boundary conditions in molecular dynamics simulations, Comput. Mater. Sci., in press.
[24] G.J. Wagner, E.G. Karpov, W.K. Liu, Molecular dynamics boundary conditions for regular crystal lattices, Comput. Methods Appl. Mech. Engrg., in this issue.
[25] J.D. Doll, D.R. Dion, Generalized Langevin equation approach for atom/solid-surface scattering: numerical techniques for gaussian generalized Langevin dynamics, J. Chem. Phys. 65 (1976) 3762–3766.
[26] S.A. Adelman, J.D. Doll, Generalized Langevin equation approach for atom/solid-surface scattering: general formulation for classical scattering off harmonic solids, J. Chem. Phys. 64 (1976) 2375–2388.
[27] W. Cai, M. DeKoning, V.V. Bulatov, S. Yip, Minimizing boundary reflections in coupled-domain simulations, Phys. Rev. Lett. 85 (2000) 3213–3216.
[28] W. E, Z.Y. Huang, A dynamic atomistic-continuum method for the simulation of crystalline materials, J. Comput. Phys. 182 (2002) 234–261.
[29] T. Hughes, G. Feijoo, L. Mazzei, J. Quincy, The variational multiscale method—a paradigm for computational mechanics, Comput. Methods Appl. Mech. Engrg. 166 (1998) 3–24.
[30] W.K. Liu, R. Uras, Y. Chen, Enrichment of the finite element method with the reproducing kernel particle method, J. Appl. Mech. 64 (1997) 861–870.
[31] G.J. Wagner, W.K. Liu, Hierarchical enrichment for bridging scales and meshfree boundary conditions, Int. J. Numer. Methods Engrg. 50 (2001) 507–524.
[32] L.T. Zhang, G.J. Wagner, W.K. Liu, A parallel meshfree method with boundary enrichment for large-scale cfd, J. Comput. Phys. 176 (2002) 483–506.
[33] D. Qian, Ph.D. Thesis, Northwestern University.
[34] H. Kadowaki, W.K. Liu, Multiscale analysis of heterogeneous materials, Comput. Methods Appl. Mech. Engrg., in this issue.
[35] D. Qian, G.J. Wagner, W.K. Liu, A multi-scale projection method for the analysis of carbon nanotubes, Comput. Methods Appl. Mech. Engrg., in this issue.
[36] W.K. Liu, Development of mixed time partition procedures for thermal analysis of structures, Int. J. Numer. Methods Engrg. 19 (1983) 125–140.
[37] W.K. Liu, T. Belytschko, Mixed-time implicit–explicit finite elements for transient analysis, Comput. Struct. 15 (1982) 445–450.